ADA053330

(8)

FINAL REPORT

ON

DEVELOPMENT OF BASIC PROCESSING TECHNOLOGY

FOR

BEARING QUALITY SILICON NITRIDE BALLS

DECEMBER 1977

Contributors:

H. M. Dalal
J. W. Rosenlieb
L. B. Sibley

U.S. NAVY CONTRACT NO. N00019-76-C-0684

SKF REPORT NO. AL77T057

SKF CODE NO. LC398

SKF REG. 414 2

D D C

RECEIVED

APR 28 1978

B

SUBMITTED TO:

U. S. DEPARTMENT OF THE NAVY
NAVAL AIR SYSTEMS COMMAND
CODE AIR 310C (JPI)
WASHINGTON, D.C. 20360

RESEARCH LABORATORY
SKF INDUSTRIES, INC.
ENGINEERING AND RESEARCH CENTER
KING OF PRUSSIA, PA.

9 FINAL REPORT

ON

DEVELOPMENT OF BASIC PROCESSING TECHNOLOGY

6

FOR

BEARING QUALITY SILICON NITRIDE BALLS

11 DECEMBER 1977

12 67p.

Contributors:

20 H. M. Dalal,
J. W. Rosenlieb
L. B. Sibley

Prepared: Harish M Dalal

Approved:

Released:

15

U.S. Navy Contract No. N00019-76-C-0684
14 SKF Report No. AL77T057
SKF Code No. LC398
SKF Reg. 414 2

SUBMITTED TO:

U. S. DEPARTMENT OF THE NAVY
NAVAL AIR SYSTEMS COMMAND
CODE AIR 310C (JPI)
WASHINGTON, D.C. 20360

DDC

RECEIVED

APR 28 1978

B

RESEARCH LABORATORY
SKF INDUSTRIES, INC.
ENGINEERING AND RESEARCH CENTER
KING OF PRUSSIA, PA.

400 241

TABLE OF CONTENTS

ACCESSION for

NTIS	White Section ☑
DDC	Buff Section ☐
UNANNOUNCED	☐
JUSTIFICATION	

BY
DISTRIBUTION/AVAILABILITY CODES

Dist.   AVAIL. and/or SPECIAL

A

RESEARCH LABORATORY SKF INDUSTRIES, INC.

LIST OF TABLES

RESEARCH LABORATORY SKF INDUSTRIES, INC.

LIST OF FIGURES

LIST OF FIGURES (CONTINUED)

RESEARCH LABORATORY **SKF** INDUSTRIES, INC.

AL77T057

DEVELOPMENT OF BASIC PROCESSING TECHNOLOGY
FOR BEARING QUALITY SILICON NITRIDE BALLS

SUMMARY

This is the Final Report on the Development of Basic Processing Technology for Bearing Quality Silicon Nitride Balls. Substantial rolling contact fatigue life data generated on balls has demonstrated the potential of this material for reliable long life. To provide a cost-effective manufacturing technology, fabrication of rough spheres directly from silicon nitride pwoder was undertaken. These were finished into 17.5mm size balls to generate rolling contact fatigue life data comparable to that available in the literature. The work was conducted under Contract N00019-76-C-0684.

This report is written in four parts.

Part I discusses the techniques of forming rough spheres, and the subsequent machining operations to obtain finished balls.

Part II presents the results of physical property and microstructural evaluations of the selected materials.

Part III presents the results of the non-destructive techniques evaluated for detection of material processing and fabrication related defects in silicon nitride balls.

Part IV discusses the rolling four-ball fatigue life data obtained.

RESEARCH LABORATORY **SKF** INDUSTRIES, INC.

CONCLUSIONS

1. Hot-pressed silicon nitride can be pressed into rough bearing shapes such as balls having just as good bearing life properties as bearing parts cut from large billets.

2. Material quality inspection techniques such as ultrasonics, acoustic microscopy and Krypton exposure correlate well with strength and microhardness properties and have inherent capabilities of detecting material defects in silicon nitride such as inclusions and porosity that are detrimental to bearing performance.

3. Norton's MgO-bonded hot-pressed NORALIDE NC132 gives consistantly superior wear and fatigue life performance in rolling contact, when properly finished. Ceradyne's Y_2O_3-bonded hot-pressed CERALLOY 147Y wore excessively at high element test stress conditions, but still had an inherent fatigue spalling life superior to M-50 bearing steel in this test. GTE Sylvania's pressureless sintered silicon nitride wore excessively and spalled at very early life, due to its relatively high porosity content (2% by volume).

RESEARCH LABORATORY SKF INDUSTRIES, INC.

PART I

FABRICATION OF ROUGH SPHERES AND FINISHED BALLS

1. Introduction

    Until recently the fabrication of a fully dense silicon
nitride part free of bearing life degrading defects con-
sisted of producing a fully dense billet and machining
the desired part from it. Due to the extreme hardness of
silicon nitride, this is a tedious and expensive process.
This has prompted several investigators to evaluate methods
by which fully dense bearing quality parts can be fabri-
cated to near net shapes. Two techniques developed to
fabricate fully dense parts directly from silicon nitride
powder were selected for this program. The first is a
conventional hot pressing technique in which silicon nitride
powder mixed with suitable type and quantity of binder
is pressed into a sphere shape at high temperatures (1650°-
1750°C) in graphite dies. The second, a pressureless
sintered product, is a more recent development (1)* in which
silicon nitride powder is blended with suitable type and
quantity of binder and then cold pressed to shape either
by uniaxial pressure using metal dies or by isostatic
pressure using polyurethane molds. The cold pressed parts
are then sintered at high temperature without application
of pressure as in hot pressing. These are referred to
as pressureless sintered parts in contrast to reaction sin-
tered parts in which the sintering and nitridation of
metallic silicon compacts into silicon nitride are performed
simultaneously.

    In the present program hot pressed rough spheres were
obtained from Norton and Ceradyne, and those fabricated
by pressureless sintering were obtained from GTE Sylvania.

2. Fabrication of Rough Spheres and Finished Balls

    The analyses of the silicon nitride powders used by
the three selected material suppliers are described, to
the extent available, in Tables 1-3. The physical charac-
teristics of individual rough spheres manufactured by
Norton and Ceradyne are listed in Tables 4 and 5. Figure
1 provides a visual comparison of the rough spheres received
from each of the three sources.

---

*Numbers in parentheses refer to the list of references
at the end of this report.

RESEARCH LABORATORY SKF INDUSTRIES, INC.

A total of sixteen experimentally hot pressed rough spheres were provided by Norton Company at no charge for this program. The composition of the material conforms to the commercial NORALIDE NC132 grade. As seen in Table 5 and Figure 1, these first attempt rough spheres were out-of-round and had a large equatorial band which prohibited use of a conventional processing cycle to finish them into bearing balls. Attempts to remove the equatorial band by tumbling was found to be either extremely slow or unreliable in avoiding harmful surface damage. Ultrasonic machining was then tried and this produced significantly faster material removal rate and provided good control on the surface and geometric quality of the machined sphere. The rough spheres from Group 1 in Table 5 were therefore rounded by ultrasonically machining between two hemispherical cavities. Since the process is of significant value to machining ceramic parts, a brief explanation of the technique and its capabilities are given at the end of this section. Once the out-of-roundness of the rough Norton spheres was reduced to <0.1 mm they could be readily subjected to the lapping procedure previously developed at SKF (2) to produce finished balls having an out-of-roundness of <0.62 μm and a surface roughness of <0.03 μm AA, free of bearing fatigue life degrading surface defects.

The fifty rough spheres procured from Ceradyne were fabricated from 85 w/o CP85 silicon nitride powder, supplied by Kawecki Berylco, and 15 w/o Y_2O_3 and is classified as Ceralloy 147Y. The geometric quality of these spheres was good enough to subject them directly to conventional ball processing. There appeared to be some spot-to-spot variation in the machinability of the material as considerably more extra care was required during the processing than in the case of the Norton spheres to produce the same degree of roundness in the final lapping step. The difference in the lapping response of the materials is related to the differences in the microstructures of these materials.

The GTE Sylvania rough spheres were produced by cold isostatic pressing followed by sintering. The geometric quality of these rough spheres was also very good. A large proportion of these balls had a mottled appearance consisting of light and dark grey areas (Figure 2). During the course of finishing it was found that the light area machined significantly faster than the dark area preventing the balls from rounding to <0.62 μm. Talyrond trace on a lapped ball (Figure 3) shows the surface unevenness.

RESEARCH LABORATORY SKF INDUSTRIES, INC.

The lighter regions contain larger pores than the darker ones. The pores in the lighter region were generally filled with unsintered Si_3N_4 particles whereas the pores in the darker region contain relatively fewer unsintered grains. The bonding of the Si_3N_4 grains in general were poorer in the lighter areas compared to the darker ones. These differences are evident in the scanning electron micrographs shown in Figure 4.

3.   Ultrasonic Machining

Ultrasonic machining was found to be uniquely applicable for shaping of hard ceramics. The method is analogous to grit blasting in which abrasive grains are propelled to the surface to be machined by fluid pressure. The basic set-up for ultrasonic machining is shown schematically in Figure 5. The tool is vibrated at a frequency of 20,000 strokes per second by an ultrasonic transducer. A slurry containing 30-50 weight percent of a suitable abrasive is allowed to flow between the tool and the workpiece. The clearance between the tool and the workpiece is only slightly greater than the size of the abrasive being used. Cavitation of the liquid due to the high frequency vibration of the tool generates a pumping action which helps to remove used abrasive and wear debris produced from the workpiece.

The shape cut in the workpiece is an exact copy of the shape of the tool. Figure 6 shows photographs of the set-up for ultrasonically machining a ball bearing inner ring. Photographs of tooling to produce outer rings from cylinders and to machine ball grooves in both inner and outer rings are shown in Figure 7. Material removal rate, surface roughness and dimensional accuracy to which a part can be produced by ultrasonic machining depend on the abrasive grit size.

Rough spheres have been produced from hot pressed silicon nitride cylinders using a slurry containing 50 weight percent of 240 grit silicon carbide with a material removal rate (MRR) of 1000 μm (0.040") per hour. As machined spheres using ultrasonics had an average surface roughness of 0.6 μm AA (24 μin AA) and an out-of-roundness of 40 μm (0.0016"). Improvement in surface finish and out-of-roundness is possible by using a smaller grit size, but with an accompanying reduction in material removal rate.

RESEARCH LABORATORY SKF INDUSTRIES. INC.

Grooves have been machined into silicon nitride rings using two machining steps. In the first step a slurry containing 50 weight percent of 320 grit silicon carbide was used to rough machine the groove. In the second step a slurry containing 30 weight percent of 600 grit silicon carbide was used. The average surface roughness of the groove was 0.3 μm AA (12 μin AA). This demonstrates that by adjusting grit size, concentration and type one can use ultrasonic energy to either rough machine to shape or finish polish ceramic surfaces.

The tooling shown in Figure 7 was used to ultrasonically machine the rings of the all-silicon-nitride ball bearing shown in Figures 8 and 9. This ceramic bearing manufacturing process development demonstrates a greatly increased MRR over conventional diamond grinding with greatly reduced cost of tooling and abrasives for producing special double curved bearing race and roller surfaces. The process can be readily scaled-up for production to produce damage free surfaces found to be important to rolling contact fatigue performance (3).

PART II

PHYSICAL PROPERTIES AND MICROSTRUCTURAL EVALUATION

To evaluate the physical properties and microstructures of the hot pressed materials, sections were made parallel to the equator. The rough spheres produced by isostatic pressing do not possess an equator so random sections were taken from these spheres. Physical properties were evaluated using diamond pyramid (Vicker's) microhardness measurements under 500 gram load, and strength measurements using a biaxial stress fixture. Microstructural evaluation was made using optical and scanning electron microscopy.

1.   Microhardness Measurements

During hot pressing the conditions used can produce a pressure gradient across the diameter of the ram. Depending on the hot pressing temperature used, additive type and content and degree of pressure gradient there could be a density gradient across the diameter of the pressed sphere in a plane perpendicular to the pressing direction. Sections of the Norton and Ceradyne spheres were made to determine any density gradient present. Results of microhardness measurements made with a diamond pyramid indentor using a 500 gram load are given in Table 6. A few random measurements made on a section from a GTE Sylvania silicon nitride sphere and a section from a billet of NORALIDE NC132 grade silicon nitride are also reported for comparison.

Measurements on the section from a Norton sphere shows good uniformity of hardness across the diameter. The hardness on the sphere section is seen to be higher than that of an older NORALIDE NC132 grade billet material. Microhardness measurements across the section from a Ceradyne sphere reveals a large hardness drop at certain random locations. The harder regions in this material are comparable in hardness to that of the Norton material. The softer regions contain a glassy phase revealed by plane polarized light microscopy discussed in this section. These softer (weaker) regions fracture under high tensile stresses produced at the edge of the contact region (4) and cause wear of the rolling track as discussed in Part IV. Microhardness values obtained at four locations on a section from a GTE Sylvania sphere are significantly lower than the hot pressed material.

RESEARCH LABORATORY SKF INDUSTRIES, INC.

2. Strength Measurements

Strength values for the three materials were obtained
by Dr. J. D. Venables of Martin Marietta using a biaxial
stress fixture (5,6). This method avoids failures due
to edge flaws encountered in three-point and four-point
measurements. Disc shaped specimens were fabricated from
the rough spheres. The strength values are comparable
to those measured by three-point bending tests on the same
material.

The GTE Sylvania material , having the lowest hardness
and containing a significant amount of porosity, has the
lowest strength of 0.43 GPa (62 ksi). The Ceradyne material
has the next highest strength of 0.56 GPa (82 ksi).
Norton material showed the highest strength of 0.99 GPa
(144 ksi).

Fractographs made with a SEM are shown in Figures
10-12. Porosity is clearly responsible for fracture initia-
tion in the GTE Sylvania sample. A high magnification view
of the pore surface does not reveal unsintered silicon
nitride grains, probably since they may have been dislodged
in the fracture process. In the Ceradyne material a cluster
of second phase particles (free Si) was responsible for
fracture initiation. A high magnification view of the frac-
ture surface shows presence of a large volume fraction
of the second phase particles. Fracture initiation in
the Norton material appears to have occurred at surface
scratches. The degree of material cleanliness and absence
of porosity explain the high strength value obtained for
the Norton's NORALIDE NC132 grade silicon nitride.

3. Microstructural Examinations

Microstructures of the three materials were studied
with the help of optical and scanning electron microscopes.
Both unpolarized and plane polarized light were used during
optical microscopy. Since the optical properties of the
various phases present in the three silicon nitride compo-
sitions are not known, it was not possible to determine the
type of phase seen on the micrograph. The results are re-
ported to document the preliminary observations on the
optical characteristics of the various phases observed.

Optical and scanning electron micrographs of the three compositions are shown in Figures 13 - 15. The GTE Sylvania material contained an estimated 5 v/o (3 v/o large + 2 v/o very fine) second phase inclusions (Figure 13a). The large inclusions remained dark when viewed in plane polarized light (Figure 13b). Porosity level is estimated to be 2 v/o (Figure 13c). Backscattered electron image (Figure 13d) at a high magnification reveals a needle-like structure. These represent α-Si_3N_4 needles that form within the amorphous Si_3N_4 particles during initial crystallization (7).

The Ceradyne material also contained large and small second phase inclusions (Figure 14a). The large ones turned dark in plane polarized light (Figure 14b). The plane polarized light micrograph also reveals a patch of glassy material. Some areas in the material contained very large patches of glassy material (Figure 14c). Chemical analysis conducted using a wavelength spectrometer indicated that the large inclusions are rich in silicon and therefore likely to be free silicon. The glassy phase is richer in yttrium than the matrix and therefore likely to be yttrium silicon oxynitride ($Y_2Si_3O_3N_4$) reported to be present in this material (1). Yttrium rich inclusions were also found (Figure 14d). The compound form of the latter yttrium rich inclusion was not established.

The NORALIDE NC132 grade silicon nitride used in the Norton spheres is relatively very clean compared to the previous two materials. Only a few very small second phase inclusions consisting of free silicon associated with metallic (bright) particles were found (Figure 15a). This is in agreement with Norton's own findings (8). Plane polarized light view of the same area (Figure 15b) shows a fine dispersion of glassy phase. For comparison a micrograph of an older sample of NORALIDE NC132 grade silicon nitride is given (Figure 15c). The inclusion content of the older material is larger in quantity and size compared to the present batch, suggesting a considerable improvement in processing technique. Scanning electron microscopy of the structure did not reveal anything more than the familiar distribution of W-rich inclusions in Si_3N_4 matrix found in NC132 materials.

RESEARCH LABORATORY **SKF** INDUSTRIES. INC.

PART III

EVALUATION OF NON-DESTRUCTIVE FLAW DETECTION TECHNIQUES

A cursory examination of four non-destructive techniques to detect material and/or fabrication related flaws was conducted. These are:

1. Ultrasonic Inspection
2. Acoustic Microscopy
3. Krypton Exposure Technique (KET)
4. Surface Residual Stress Measurement using X-ray Diffraction

1. Ultrasonic Inspection

This work was performed at TRW, Inc., using the instrumentation and techniques developed under NAVAIR contracts (9,10). Examinations were conducted using 45 MHz longitudinal and shear waves. Longitudinal waves were used to examine density variation from point-to-point. Shear waves, due to their shorter wavelength(hence better resolution), were used for detection of porosity and inclusions.

Six sections having a thickness of 2 ± 0.05 mm were provided for this study. These are:

a) NORALIDE NC132 billet section
b) NORALIDE NC132 billet section containing microhardness indentations made at 1, 0.5, 0.3 and 0.2 kg loads.
c) NORALIDE NC132 powder processed ball section made perpendicular to the equator
d) Ceralloy 147Y powder processed ball section made perpendicular to the equator.
e) Ceralloy 147Y powder processed ball section made parallel to the equator.
f) GTE Sylvania powder processed ball section.

According to McLean, et al (11) the density variation with velocity for silicon nitride is 0.2 g/cc/km/s. The signal was allowed to reflect four times before recording its time of flight through the material at each point to improve the resolution in velocity measurements and thereby the resolution in density variation. The available accuracy in the time of flight measurement is $\pm$ 8 nanoseconds (8×10^{-9} secs.). In the present case this corresponds to a resolution in density of $\pm$ 0.001 g/cc.

The velocity readings taken and equivalent density values at five points on each of the six specimens are listed in Table 7. Statistical evaluation of the measurements shows that the density variations measured on the two Ceradyne samples are significant whereas those measured on the other four samples are within experimental error. The greater density variation found in the Ceradyne samples is in conformance with the greater variation in microhardness values obtained on the same material.

Attempts to detect internal flaws in the different materials or microhardness indentations on the NORALIDE NC132 billet specimen were unsuccessful. This is considered to be largely due to inappropriateness of the available transducer for the thin samples used. A short water path of 2 cms. was used to minimize signal attenuation and thereby loss in sensitivity. The available transducer, having a focal length of 63.5 mm (2.5 in.) in water, was designed to be used with 8.25 mm (0.25 in) thick specimens. The use of 2 mm thick spcimens in the present study did not permit the acoustic beam to focus within the specimen and therefore the examination was conducted at less than optimum conditions. The small specimen thickness was essential to be able to examine the material of the rough spheres as close to the edges as possible without interference from the curvature of the sphere.

Surface microhardness indentations are not detectable by C-scan technique using either longitudinal or shear wave modes due to the presence of a 40 µm dead band present near the top and bottom specimen surfaces. This is caused due to the interference between incident and reflected beams. The maximum depth of the microhardness indentation introduced at 1 kg is 4 µm. Loss-of-back-reflection intensity measurements were made using longitudinal waves and placing the indented surface facing down. The microhardness indentations were not detectable. It is certain that use of a proper transducer can improve the sensitivity of the shear

-11-

RESEARCH LABORATORY **5KF** INDUSTRIES. INC.

wave mode considerably. Use of the surface wave technique, presently being developed at TRW, Inc. under a NAVAIR contract, would enable detection of surface flaws such as the microhardness indentations. The indentations are much larger than the largest tolerable surface flaw or one that would be generated by slightly abusive fabrication methods. The ultimate test of a surface flaw detection technique would lie in its ability to detect significantly smaller surface flaws of the type shown in Figure 16 produced on a ball surface by an improper lapping procedure. Removal of this damaged surface material produced a minimum improvement in the L_{10} life of the balls from 7.55×10^6 revs. to 36.7×10^6 revs. (2).

2.   Acoustic Microscopy

This is a desirable modification of the C-scan ultrasonic inspection technique. The desirability is in the fact that an image similar to that of an optical microscope is produced, simplifying interpretation of the information. The commercial model 'SONOMICROSCOPE 100' was used for this study. It uses 100 MHz shear waves and is capable of producing a direct image of the transmitted acoustic signal showing the acoustically different features encountered in the volume through which the beam was transmitted. It also produces acoustic interference images similar to the type of image produced in optical interference microscopy. Analysis of the fringe positions provides quantitative information on a microscopic scale regarding the elastic properties of the regions within an insonified volume. The conversion of the acoustic signal into a real time image on a television monitor is done by means of a high resolution laser microphone (12, 13).

The technique depends for its detection on the degree of acoustic mismatch between the matrix and the flaw. Acoustic impedance (Z) is defined as the product of density (ρ) and acoustic velocity in the material (v) which in turn is a function of elastic modulus and density.

$$Z = \rho v$$

The degree of acoustic mismatch is defined as

$$\frac{Z - Zm}{Z + Zm}$$

where Z = acoustic impedance of flaw

Zm= acoustic impedance of matrix

Since the stress raising ability of a flaw and acoustic mismatch are both in some way functions of the degree of elastic mismatch between the flaw and the matrix, it is evident that this technique would detect the most strength degrading flaws first. This is a very desirable capability of the technique.

The resolution of the acoustic microscope is approximately one wavelength of sound in the material being investigated or approximately 50 μm in hot pressed silicon nitride. The sensitivity is estimated to be one-fifth this size. Acoustic micrographs of the three silicon nitride materials used in this program are shown in Figures 17-19, as obtained at Sonoscan, Inc.

An image of an acoustically homogeneous material would be monotonous and the interference image would show straight interference lines. This is seen to be true of the NORALIDE NC132 material (Figure 17). The acoustic micrograph of Ceralloy 147Y (Figure 18) shows regions that are both lighter and darker than the matrix. The lighter features are inclusions with a lower acoustic attenuation than the matrix whereas the darker regions are regions with higher attenuation and are likely to be fine pores in the material. The shift of the interference fringes to the left in the light appearing inclusions is indicative of lower acoustic velocity in it compared to the matrix. Acoustic micrograph of the GTE Sylvania material (Figure 19) shows larger light and dark regions indicative of presence of larger size inclusions and pores in the material. The presence of porosity in the GTE Sylvania material has been established by other methods of examination. Fractographs on the Ceralloy 147Y material shows presence of faceted grains which could occur either due to a transgranular mode of fracture or presence of porosity. Occurrence of dark regions on the acoustic micrograph indicates that some of the unbonded grain surfaces visible on the fractograph must be due to the presence of porosity.

Regions of low acoustic velocity in Ceralloy 147Y found in 45 MHz inspection were also detected during acoustic microscopy inspection.

3.   Krypton Exposure Technique (KET)

This is a relatively new non-destructive test technique for detection of surface flaws. In principle it is similar to the conventional dye penetrant method of detecting surface flaws where the conventional dye is replaced by radioactive Krypton (Kr^{85}). The latter is a fission by-product of U^{235} produced in nuclear fission reactors controlled by the U. S. Government.

Parts to be examined are placed in a vacuum chamber which is evacuated to a pressure of 10 μm of Hg. The chamber is then backfilled with Kr gas containing about 5% radioactive Kr, the rest being stable Kr. The parts are allowed to soak in the gas for about one hour. The soaked parts are removed from the chamber and coated with a photographic emulsion. The emulsion is exposed for a period of 24 hours and then developed for detection of surface flaws where Kr^{85} embedded during the soaking operation. Several precautions must be observed in using KET for detection of surface flaws. Surfaces of the parts should be thoroughly cleaned as dirt can act as a trap to Kr^{85}.

The characteristics of the photographic emulsion used are similar to dental X-ray film. Energy of the β-radiation emitted by Kr^{85} can be completely absorbed by an emulsion thickness of 80 μm which is therefore the optimum thickness. Emulsion thicknesses much smaller than 80 μm will lose a significant amount of energy through transmission. Thicker coatings will make detection of exposed areas more difficult due to the presence of an overlayer of unexposed emulsion. In practice, attempts are made to control the thickness of the photographic emulsion between 50 and 80 μm. In parts containing fillets and under-cuts this can be achieved by resorting to a mist spray technique of applying the emulsion instead of dipping the parts in the emulsion.

The sensitivity of KET is limited only by the grain size of the emulsion film, so that it can be expected that a maximum sensitivity of about 4 μm will be obtained. For an initial evaluation of this technique one GTE Sylvania ball and one Norton finished ball were examined at QUAL-X, Inc. The GTE Sylvania ball, having a light color, was processed as is. The darker colored Norton ball was coated with TiO_2 to improve the visibility of the exposed areas. This was necessary since it was found difficult to peel the emulsion off the ball surface for examination without disturbing or breaking it. The dark color of the ball made it difficult to see any dark exposed areas on the overlaying film.

The dark spots on the GTE Sylvania balls shown in Figure 21 indicate the presence of surface porosity known to exist in this material from other examinations. No indications are visible on the Norton ball. The technique has a definite advantage in that it can examine the entire surface simultaneously compared to other techniques where point-to-point inspection is required. For the technique's success as a routine inspection tool for bearing components, it is necessary to develop better methods for application and removal of photographic emulsion for examination. Adequate knowledge of the correlation between the presence of an indication and its size with the type and size of the surface flaw appears to be lacking at the present time.

4. Surface Residual Stress Measurements by X-ray Diffraction

The majority of the rolling contact fatigue failures encountered in silicon nitride are surface initiated (14, 15, 16, 17). These surface initiated failures can be significantly affected by the type and magnitude of surface residual stresses produced during fabrication of a component. Effect of processing parameters on the strength and fatigue life of metals has been long established (18,19). Adaptation of the measurement technique (20) to silicon nitride would provide a means of devising fabrication processes to generate surface compressive stresses.

Calibration of the technique using the established procedure (20) was conducted with the help of a beam provided by Norton and a four-point bending attachment for the X-ray machine. The as-received beams were finished to 10 x 1.5 x 0.2 cm and strain gaged as shown in Figure 20. The [720] β-Si_3N_4 peak located at 2θ angle of 147.17 degrees with copper radiation (21) and a ψ-rotation of 45° were used. The stress factor under these conditions is calculated to be 198 ksi/degree. The measured value of the ratio $(E/1+\upsilon)$ = 259.25 GPa (37.6×10^6 psi) where E is the elastic modulus of the surface material and υ its Poisson's ratio. Using a value of υ = 0.25 the value of E is calculated to be 324.07 GPa (47×10^6 psi). This is in good agreement with the literature value of 310.26 GPa (45×10^6 psi).

-15-

PART IV

ROLLING FOUR-BALL FATIGUE TESTS

The experimental evaluation of the fatigue life of the three groups of Si_3N_4 balls was performed on rolling four-ball testers. The test series was designed to determine the relative differences in the fatigue life of the three groups and provide a comparison of the lives with that previously obtained for CVM M-50 steel balls and NC132 grade silicon nitride balls manufactured from a hot pressed billet (2).

Rolling Four-Ball Tester & Test Procedure

A schematic of the rolling four-ball tester is presented in Figure 22. In the four-ball tester, the test specimen, i.e. the spindle ball, is held in a vertical arbor against three support balls which orbit the spindle ball in a stationary cup race. The spindle ball is fixed in position with respect to the rotating arbor by a spring loader/plunger pressed against a flat surface ground on the top of the spindle ball and the friction between the cone machined in the end of the arbor and the ball spherical surface. Two flats are machined on each spindle ball diametrically opposite each other; thus, each ball is tested twice, i.e. each end is considered as one test specimen.

The support balls are positioned in the cup race 120° apart and held in this relative position by a brass cage or separator. The positioning of the cup concentric with the spindle axis insures equal loading of the support balls and identical Hertzian stress at the three contact points between the spindle (test) ball and the support balls. The contact angle of the assembly is controlled by the race design in the cup and the support and test ball sizes, see Figure 23. The load, which determines the Hertz stress at the contact points between the balls, is applied through the spindle by a dead weight lever system. The spindle is driven by a constant speed AC motor through a pulley and belt drive system. The spindle speed can be varied by changing the ratio of the drive to driven pulley diameters.

Lubrication is provided by a once-through, drip-feed system. The oil is fed into the bottom of the cup and flows out of the top thus maintaining a copious quantity of oil in the cup for lubrication of the contacts. A vibraswitch mounted on the cup support table automatically turns the drive motor off and stops the testing at the initiation of a spalling failure.

Prior to the initiation of each test, the concentricity of the cup race with respect to the spindle axis was determined with the operating load applied and any necessary adjustments made. The cup race was visually examined for damage, and if damage was present the cup was replaced. The spindle ball, support balls and cup were cleaned before assembly and coated with oil. After assembly and prior to starting the drive motor, a copious supply of oil was injected into the cup while the spindle was rotated by hand. This was performed to prevent any chance of wear at startup due to lack of lubricant. Each test was performed until a spall or wear failure occurred on the spindle ball or to a pre-established time up. Following each motor stoppage due to the vibraswitch, all balls were inspected. If the test ball had failed, the test was terminated. If a support ball had failed, all three support balls were replaced and the test continued.

A lubricant meeting MIL-L-23699 specifications was used in all tests and supplied at a rate of 3-6 drops per minute. The spindle balls were 17.5 mm in diameter and the support balls were machined from M-50 steel to 12.7mm diameter. The spindle speed and load, the calculated maximum Hertz stress, and the calculated Lundberg-Palmgren L_{10} life for each test condition used are presented in Table 8.

Test Results and Discussion

The testing was initiated on the Ceralloy 147Y balls which had been finished using a previously established procedure (2) consisting of rough lapping with 15 μm diamond followed by polishing with E-330 grade Al_2O_3. The same process was used to finish all the balls tested on this program.

To permit a direct comparison between this material and previously tested Si_3N_4 balls, testing was initiated with a load of 1470N(333 lbs) which produces a maximum Hertz stress of 5.5 GPa (800 ksi). A spindle speed of 10,000 rpm was used. Four test machines were used on this program.

Shortly after starting the testing, excessive wear was noted by discoloration of the lubricant which turned black. Since the wear occurred within a short test period, possibility of test machine and lubrication problems were considered. Therefore, each machine was checked for alignment and proper load application. In addition comparison balls from a lot tested on a previous contract (20) were run for several hours prior to, and in some cases following, the Ceralloy ball tests. In all cases the comparison ball ran without wear; thus, indicating that the wear failures were material related.

RESEARCH LABORATORY **SKF** INDUSTRIES. INC.

Considering that the material may still be suitable for
bearings, where the Hertz stress would be lower, (the exception-
ally high stress loads are applied in the four ball tests to
reduce the test time requirement) the Hertz stress value was
decreased in steps over the remaining tests to a minimum value
of 3.4 GPa (500 ksi). The test stress, test time, and results
of each test are presented in Table 9. Wear rate decreased
with load but wear never stopped completely even at the lowest
stress level. This prevented obtaining classical spalling fatigue
data on the material except possibly in two tests where spalling
failures occurred with minimal wear (Tests No. C-11 and C-20).
Wear at maximum Hertz stresses of 3.4 and 4.1 GPa (500 & 600 ksi)
was intermittent whereas it was continuous at 4.7 and 5.5 GPa
(680 & 800 ksi) maximum Hertz stresses. In the intermittent
mode the rolling track would first glaze and acquire a shine.
The glazed material would then peel off suddenly and the process
repeated itself. It was also obvious during the testing of
Ceralloy 147Y balls that the wear would often start as pitting
or microspalling at the light colored (grey) areas which were
randomly distributed over the surface of the ball.

As a result of the excessive wear experienced during the
rolling four-ball tests even at the lowest stress values, the
Ceralloy 147Y material containing acoustic microscopically
detected porosity is not considered to be a good candidate for
rolling bearing applications. An estimate of the inherent spal-
ling fatigue life of this type of material can be obtained how-
ever by using only the spalling failure lives in Tests C-11 and
counting all other tests in which wear occurred as suspension.

Pressureless sintered balls made by GTE Sylvania were tested
next. These balls were light gray in color and contained about
2 v/o porosity evenly distributed through the volume.

The testing of these balls was also initiated at a stress
level of 5.5 GPa (800 ksi) Hertz stress. Wear was noted by
the discoloration of the lubricant after 6 minutes of testing.
Inspection of the ball after one hour of running (vibraswitch
set in insensitive position to permit running) showed that ap-
preciable wear and several spalls had occurred. Testing was
terminated on this material after four additional test runs were
performed with Hertz stress values as low as 4.1 GPa (600 ksi)
with similar results, see Table 10. Porosity is believed to be
primarily responsible for the poor rolling contact performance
of this lot of balls. Further effort is being made at GTE
Sylvania to produce more fully dense rough spheres.

The third group of balls tested were made from NORALIDE NC132 Si_3N_4 material. By means of a 1.5 mm diameter blind hole put in the as-pressed balls it was possible to orient these balls so that the track intersected the equatorial band at two points. This allows evaluation of the relative fatigue strength of the bulk and the equatorial band materials. Because of the early wear failure experienced with the other two materials tested, these tests were initiated at a Hertz stress of 4.7 GPa (680 ksi). Since no wear failures were encountered in the initial testing of this material and the test time required to obtain a spall was long at the lower stress level, the time up life was set at 300 hrs. The Hertz stress was then increased to 5.5 GPa (800 ksi), and the test continued until failure or a time up of an additional 300 hours. This increase in **stress** was performed for two purposes 1) determine if the higher stress level would result in wear as experienced by the other two candidate materials, 2) accelerate the testing and keep the test time within the time frame of the program. The test results are presented in Table 11 which also shows the calculated equivalent test life at 5.5 GPa (800 ksi) Hertz stress and the theoretical L_{10} life.

Since all the values were considered to be quite good the NC132 material is considered to be superior to the other two test materials and is considered to be a good candidate for rolling bearing material.

The lowest test life value was 3 times the computed theoretical L_{10} life and three tracks ran for more than 33 times the computed L_{10} life without failing.

Examination of spalled NC132 balls revealed two types of spall initiation. All but one spall were normal fatigue spalls of the type shown in Figure 24. It is seen in Figure 24 that the Hertz cracks predominate at the edge of the track and move towards the center of the track as they progress. On the odd spall (Figure 25) the Hertz cracks had formed at the center of the track and ran perpendicular to the track. The spall is seen to be bounded on one side by a Hertz crack. Such Hertz cracks, running perpendicular to the track, are formed by repeated contact with a spall edge on the support balls. In most cases a spalled support ball does not cause the test ball to fail due to the indexing of the spalled region out of the contact band. None of the spalls occurred in the equatorial band region indicating absence of strength degradation in that region.

Examination of the rolling track on a Ceralloy 147Y ball shows microspalls and wear debris particles generated that cause oil discoloration during testing (Figure 26).

-19-

In order to perform a direct comparison with the NC132 material previously tested (19) the statistically evaluated L_{10} life of the NORALIDE NC132 Si_3N_4 material was performed using the maximum likelihood technique. The median unbiased L_{10} life is presented in Table 12 along with the L_{10} life of M-50 steel balls and similarly finished silicon nitride balls tested in (19).

Since the steel balls were tested at a lower Hertz stress value than the Si_3N_4 balls a direct comparison of the estimated L_{10} life values cannot be made. To obtain a relative evaluation of the two materials the ratios of their estimated L_{10} life to calculated theoretical life must be made. The M-50 ratio is 0.112 and the ratio of the NC132 material is 4.72. A comparison of these two values indicates that the NC132 Si_3N_4 out performed the M-50 steel by a factor of 42. A similar maximum likelihood analysis of the inherent fatigue life of Ceradyne 147Y is also given in Table 12, showing good fatigue performance compared to M-50 steel.

It must be recognized that the estimated L_{10} life results based on small test groups are particularly sensitive to a single failure if there is wide scatter in individual test life data. In addition, the high contact stress levels used in the rolling four-ball tests, compared to the lower contact stresses in ball and roller bearing applications, affect materials having different hardness and ductility, such as steels and ceramics, in quite different ways. Therefore, the life estimates obtained must be considered as indicators of life and not as engineering values.

LIST OF REFERENCES

1. Rowcliffe, D. J. and Jorgensen, P. J., "Sintering of Silicon Nitride," Proceedings: Workshop on Ceramics for Advanced Heat Engines, sponsored by ERDA, pp. 191, Orlando, Florida, (1977).

2. Dalal, H. M., et al, "Effect of Lapping Parameters on Generation of Damage on Silicon Nitride Ball Surfaces," Final Report, Naval Air Systems Command Contract No. N00019-76-C-0147, SKF Report No. AL76T026 (1976).

3. Robare, M. W. and Richerson, D. V., "Rotor Blade Machining Development," ARPA-NAVSEA/AIRESEARCH Ceramic Gas Turbine Engine Demonstration Program Review, Maine Maritime Academy, Castine, Maine (1977).

4. Timoshenko, S. and Goodier, J. N., Theory of Elasticity, New York, McGraw Hill (1951).

5. ASTM Test #F394-74T, Annual Book of ASTM Standards, Part 43, pp. 758 (1975).

6. J. B. Waxhtman, W. Capps and J. Mandel, "Biaxial Flexure Tests of Ceramic Substrates," J. Matls. 7, 188 (1972).

7. Kleiner, R. N., GTE Sylvania, Ceramics Research Division, Towanda, Pa., Private Communications.

8. Baumgartner, H. R. and Richerson, R.W., "Inclusion Effects on the Strength of Hot Pressed Silicon Nitride," in Fracture Mechanics of Ceramics, pp. 367, Plenum (1973).

9. Derkacs, T., et al, "Non-Destructive Evaluation of Ceramics," Final Report on Naval Air Development Center Contract No. N00019-75-C-0238,(July 1976).

10. Derkacs, T., et al, "Ultrasonic Inspection of Ceramics Containing Small Flaws," Final Report on Naval Air Development Center Contract No. N62269-76-C-0948, March,(1977).

11. McLean, A. F., et al, "Brittle Materials Design, High Temperature Gas Turbine," Interim Report No. 9, AMMRC CTR 76-12,(April 1976),pp. 101.

12. Kessler, L. W., in Proceeding of the Symposium on Optical and Acoustical Micro-Electronics, Vol. 23, ed. A. Oliner Polytechic Press,(1974).

13. Bratton, R. J., Anderson, C. A. and Lange, F. F., "Ceramic Rotor Blade Development," Electric Power Research Inst.Report Contract No. RP421-1,(1976).

RESEARCH LABORATORY **SKF** INDUSTRIES, INC.

14. Baumgartner, H. R. and Cowley, P.E., "Silicon Nitride in Rolling Contact Bearings," Final Report, Air Systems Command Contract No. N00019-84-C-0157, (1975).

15. Valori, R., "Rolling Contact Fatigue of Silicon Nitride," Naval Air Propulsion Test Center Report No. NAPTC-PE-42, (August 1974).

16. Dalal, H. M., et al, "Surface Endurance and Lubrication of Silicon Nitride Ball Bearings," Final Report on U. S. Department of the Navy Contract No. N00019-75-C-0216, SKF Report No. AL75T030, (December 1975).

17. Parker, R. J. and Zaretsky, E. V., "Fatigue Life of High Speed Ball Bearings with Silicon Nitride Ba-1s," Trans. ASME, J. Lub. Technology, 97 (3), pp. 350-357 (1975).

18. Almen, J. O. and Black, P. H., "Residual Stresses and Fatigue Life in Metals," New York, McGraw Hill (1963).

19. Letner, H. R., "Residual Grinding Stresses in Hardened Steel," ASME Transactions, Vol. 77, pp. 1089 (1955).

20. Residual Stress Measurement by X-ray Deffraction, SAE Handbook Supplement HS 784a (1971).

21. Gazzara, C. P. and Reed, D., "A Computed X-ray Diffraction Powder Pattern for Alpha and Beta Silicon Nitride," Army Materials and Mechanics Research Center Report No. AMMRC TN 75-4, (April 1975).

RESEARCH LABORATORY **SKF** INDUSTRIES, INC.

TABLE 1

DATA ON GTE SYLVANIA POWDER

Type of powder: SN-502

Average particle size: 0.5 μm

Surface area: 3.5 m^2/g

Oxygen Content: 1.24 $^w/o$

% Amorphous Si_3N_4: 40

%α - Si_3N_4: 57.3

%β - Si_3N_4: 2.7

SPECTROGRAPHIC CHEMICAL ANALYSIS

Element	Approximate Percent
Al	0.002
B	0.0008
Ca	0.0008
Fe	0.001
Mg	0.0009
Mo	0.01 (ND)*
Ti	0.008 (ND)

* Not Detected

RESEARCH LABORATORY SKF INDUSTRIES, INC.

TABLE 2

DATA ON SILICON NITRIDE POWDER USED BY CERADYNE

Type of powder: AME CP85

Average particle size: 2.5 μm

% α-Si$_3$N$_4$: 90

% β- Si$_3$N$_4$: 10

Free Si : 2

Oxygen content: 2.1 ^{w}/o

Theoretical density: 3.32 gm/cc

SPECTROGRAPHIC CHEMICAL ANALYSIS

Element	Approx. Percent	Element	Approx. Percent
Si	58.0	Sr	0.035
Fe	1.3	Mo	0.028
Ca	0.34	V	0.013
Al	0.48	Cu	0.0058
Mg	0.023	Ti	0.031
Ni	0.069	Zr	0.0022
Mn	0.037	W	0.07 (ND)*
Cr	0.015	Na	0.03 (ND)
Co	0.0045	K	0.10 (ND)

*Not Detected

RESEARCH LABORATORY SKF INDUSTRIES, INC.

TABLE 3

SPECTROGRAPHIC CHEMICAL ANALYSIS OF NC132

Aluminum	0.28
Calcium	0.044
Iron	0.46
Magnesium	0.56
Titanium	0.04
Tungsten	1.3
Silicon Nitride	Balance

TABLE 4

MEASUREMENTS ON INDIVIDUAL ROUGH SPHERES FROM CERADYNE

Run No. 1827

P/N	Diameter mm (in.)	Height mm (in.)	Density gm/cc$\pm$.01
1	22.1 (.87)	22.4 (.88)	3.30
2	22.1 (.87)	22.6 (.89)	3.32
3	22.1 (.87)	22.4 (.88)	3.31
4	22.1 (.87)	22.4 (.88)	3.32
5	22.1 (.87)	22.4 (.88)	3.31
6	21.8 (.86)	22.4 (.88)	3.31
7	21.1 (.87)	22.6 (.89)	3.31
8	21.8 (.86)	22.4 (.88)	3.30
9	22.1 (.87)	22.4 (.88)	3.31
10	22.1 (.87)	22.6 (.89)	3.32
11	22.1 (.87)	22.4 (.88)	3.30
12	22.1 (.87)	22.4 (.88)	3.31
13	21.8 (.86)	22.6 (.89)	3.31
14	22.4 (.88)	22.4 (.88)	3.31
15	22.4 (.88)	22.4 (.88)	3.30
16	22.1 (.87)	22.4 (.88)	3.31
17	22.1 (.87)	22.6 (.89)	3.31
18	22.1 (.87)	22.4 (.88)	3.29
19	21.8 (.86)	22.6 (.89)	3.32

RESEARCH LABORATORY SKF INDUSTRIES, INC.

TABLE 4 (CONTINUED)

Run No. 1840

P/N	Diameter mm (in.)	Height mm (in.)	Density gm/cc±0.1
20	21.8 (.86)	22.4 (.88)	3.32
21	21.8 (.86)	22.4 (.88)	3.32
22	21.8 (.86)	22.4 (.88)	3.31
23	21.8 (.86)	22.4 (.88)	3.32
24	21.6 (.85)	22.4 (.88)	3.32
25	21.8 (.86)	22.4 (.88)	3.31
26	21.8 (.86)	22.4 (.88)	3.31
27	21.8 (.86)	22.4 (.88)	3.31
28	22.1 (.87)	22.6 (.89)	3.32
29	21.8 (.86)	22.4 (.88)	3.31
30	21.8 (.86)	22.4 (.88)	3.31
31	21.8 (.86)	22.4 (.88)	3.31
32	22.1 (.87)	22.4 (.88)	3.31
33	22.1 (.87)	22.4 (.88)	3.31
34	21.8 (.86)	22.4 (.88)	3.33
35	21.8 (.86)	22.4 (.88)	3.31
36	21.8 (.86)	22.4 (.88)	3.32
37	21.8 (.86)	22.4 (.88)	3.31
38	21.8 (.86)	22.4 (.88)	3.31
39	21.8 (.86)	22.4 (.88)	3.31
40	22.1 (.87)	22.4 (.88)	3.31
41	21.8 (.86)	22.4 (.88)	3.31

TABLE 4 (CONTINUED)

42	21.8 (.86)	22.4 (.88)	3.30
43	22.1 (.87)	22.4 (.88)	3.30
44	21.8 (.86)	22.4 (.88)	3.32
45	21.8 (.86)	22.4 (.88)	3.32
46	21.8 (.86)	22.4 (.88)	3.31
47	21.8 (.86)	22.4 (.88)	3.31
48	21.8 (.86)	22.4 (.88)	3.32
49	21.8 (.86)	22.4 (.88)	3.32
50	22.1 (.87)	22.4 (.88)	3.33

TABLE 5

MEASUREMENTS ON INDIVIDUAL HOT PRESSED NORALIDE SPHERES FROM NORTON

Group 1

Ball No.	Diameter mm (in.)	Height mm (in.)
1	18.21 (.717)	20.01 (.788)
2	18.23 (.718)	19.96 (.786)
3	18.39 (.724)	19.89 (.783)
4	18.14 (.714)	19.91 (.784)
5	18.29 (.720)	19.89 (.783)
6	18.57 (.731)	20.11 (.792)
7	18.14 (.714)	19.99 (.787)
8	18.21 (.717)	20.07 (.790)
9	18.08 (.712)	19.84 (.781)

Group 2

10	21.39 (.842)	20.57 (.810)
11	21.31 (.839)	20.52 (.808)
12	21.21 (.835)	20.68 (.814)
13	21.44 (.844)	20.50 (.807)
14	21.26 (.836)	20.60 (.811)
15	20.93 (.824)	20.45 (.805)
16	21.13 (.832)	20.42 (.804)

TABLE 6

MICROHARDNESS MEASUREMENTS

Material		1	2	3	4	5	6	7	8	9	10	11	12
Norton Billet* NC132	Diag. (μm)	25	26										
	DPH_{500} (kg/mm²)	1484	1372										
Ceradyne Sphere Cer-147Y	Diag. (μm)	24.7		25	30	25.3	26.3	25	25	25.3	24.8	27.3	27.6
	DPH_{500} (kg/mm²)	1520		1484	1030	1449	1340	1484	1484	1449	1508	1244	1217
GTE Sylvania+ Sphere	Diag. (μm)		28.3	29	27	28							
	DPH_{500} (kg/mm²)		1158	1103	1272	1183							
Norton Sphere NC132	Diag. (μm)	25.3	25	25.2	25.3	24	24.5	24.7	25.7	25	25.7		
	DPH_{500} (kg/mm²)	1449	1484	1460	1449	1610	1545	1520	1404	1484	1404		

* Sample was taken from a piece of billet available in house.

+ Only four readings were taken since the material was isostatically pressed and hence lacks directionality.

RESEARCH LABORATORY SKF INDUSTRIES, INC.

TABLE 7

POINT-TO-POINT DENSITY VARIATION MEASURED ON SIX SILICON NITRIDE SPECIMENS

	(a) NC132 Billet		(b) NC132 Billet(1)		(c) NC132 Ball(2)		(d) Cer.147Y Ball(2)		(e) Cer.147Y Ball(3)		(f) GTE Sylvania Ball	
	v (km/s)	ρ (g/cc)	v (km/s)	ρ (g/cc)	v (km/s)	ρ (g/cc)	v (km/s)	ρ (g/cc)	v (km/s)	ρ (g/cc)	v (km/s)	ρ (g/cc)
Reading No.1												
	10.98	3.265	10.84	3.237	11.45	3.357	10.84	3.237	10.62	3.194	10.16	3.103
	10.98	3.265	10.84	3.237	11.45	3.357	10.77	3.223	10.62	3.194	10.16	3.103
Reading No. 2												
	10.98	3.265	10.98	3.265	11.37	3.341	10.98	3.265	10.77	3.223	10.10	3.091
	10.98	3.265	10.98	3.265	11.45	3.357	10.84	3.237	10.77	3.223	10.03	3.077
Reading No. 3												
	10.84	3.237	10.84	3.237	11.37	3.341	10.98	3.265	10.77	3.223	9.97	3.066
	10.98	3.265	10.84	3.237	11.37	3.341	11.06	3.280	10.84	3.237	10.16	3.103
Reading No. 4												
	10.84	3.237	10.77	3.223	11.45	3.357	10.98	3.265	10.77	3.223	10.10	3.091
	10.84	3.237	10.84	3.237	11.53	3.373	11.06	3.280	10.77	3.223	10.03	3.077
Reading No. 5												
	10.84	3.237	10.84	3.237	11.53	3.373	11.30	3.328	10.77	3.223	10.03	3.077
	10.84	3.237	10.84	3.237	11.45	3.357	11.21	3.310	10.98	3.265	10.03	3.077
Average Density		3.251		3.241		3.355		3.269		3.223		3.087
Density Variation		0.028		0.042		0.032		0.105		0.071		0.037

Conversion

$10,500 \text{ m/s} = 3.17 \text{ g/cc}$

(1) Containing microhardness indentations

(2) Section perpendicular to the equator

(3) Section parallel to the equator

RESEARCH LABORATORY **SKF** INDUSTRIES. INC.

TABLE 8

VARIOUS TEST CONDITIONS APPLIED

Spindle Speed (rpm)	Applied Load (N/lbs)	Maximum Hertz Stress (GPa/ksi)	Theoretical Lundberg-Palmgren L_{10} Life (10^6 revs)
10,000	1480/333	5.5/800	7
10,000	909/204	4.7/680	30
10,000	622/140	4.1/600	93
10,000	360/81	3.4/500	481

TABLE 9

ROLLING FOUR-BALL TEST DATA ON 17.5 mm CERALLOY 147Y Si_3N_4 BALLS

Ball Track (No.)	Max. Hertz Stress (GPa/ksi)	Test Time (Hrs.)	Remarks
C-1	5.5/800	0.2	Appreciable rough uneven wear
C-2	5.5/800	0.2	Excessive wear within 12 minutes. Lowered applied load, wear continued at lower rate over next 20 hrs. when spall occurred. Comparison ball ran for 10 hrs. following test without wear.
	4.7/680	20.3	
C-3	5.5/800	61.3	Wear noted after 30 hrs. continued to wear during rest of test with microspalls or pitting occurring at high spots.
C-4	5.5/800	0.2	Wear noted within 12 min. by generation of debris. Comparison ball ran for 22 hrs. prior to test without wear occurring.
C-5	5.5/800	21.4	Wear noted after a few minutes and continued through remainder of test. Comparison ball ran for 17 hrs. prior to test without wear occurring.
C-6	4.7/680	180.0	Ran for 50 hrs. with only minor wear. Wear continued through remainder of test. Surface would become highly polished and then appear to peel.
C-7	5.5/800	7.4	Wear started within 6 min. and continued through remainder of test with microspalling or pitting occurring at light spots. Compariosn ball ran for 7.5 hrs. prior to test without wearing.
C-8	5.5/800	0.3	Wear noted after 18 minutes. Compariosn ball ran for 30 hrs. without wear. Test ball located at new position wore within 6 minutes.
	5.5/800	0.1	
C-9	4.1/600	128.0	No appreciable wear while running at 600 ksi Hertz stress for 128 hrs. After running for 97 hrs. at 680 ksi Hertz stress some microspalling or pitting occurred at light spots. After running an additional 179 hrs. at the higher stress level minor flaking or peeling occurred.
	4.7/680	97.0	
	4.7/680	179.0	

RESEARCH LABORATORY **SKF** INDUSTRIES, INC.

Table 9 Continued

C-10	4.7/680	90	After 90 hr. microspalling or pitting occurred in light areas.
C-11	4.7/680	34.7	A major spall and some microspalls occurred after 34.7 hrs. of running.
C-12	4.7/680	8.0	Observed wear after 2 hrs. Excessive wear after 8 hrs.
C-13	4.7/680	53	Observed wear after 11 hrs. Excessive wear and peeling after 53 hrs.
C-14	- - - -	- - -	End damaged, not tested
C-15	4.7/680	69	Heavy wear noted after 30 hrs. Wear continued during rest of test, peeling and pitting in light spots.
C-16	4.1/600	375	Wear noted after 17 hrs. Wear continued during remainder of test with alternate polishing and peeling. Gross wear at end of test.
C-17	4.1/600	150	Wear noted after 15 hrs. Wear continued during remainder of test with alternate polishing and peeling.
C-18	3.4/500	205	Wear noted after 4 hrs. Wear continued at slow rate through remainder of test with microspalls or pitting in light spots.
C-19	4.7/680	128	Wear noted after 8 hrs. After 68 hrs. microspalling in light spots. Wear continued through remainder of test.
C-20	4.7/680	85	Noted wear after 72 hrs. Two small spalls and heavy wear after 85 hrs.
C-21	4.1/600	85	Noted wear after 15 hrs. Continued to wear through remainder of test with alternate polishing and peeling.
C-22	3.4/500	169	Noted wear after 22 hrs. Continued with alternate polishing and peeling through remainder of test.
C-23	3.4/500	168	Minor wear, not as great as observed with other test tracks at the low Hertz stress.

TABLE 10

ROLLING FOUR-BALL TEST DATA ON 17.5 mm GTE Si_3N_4 BALLS

Ball Track (No.)	Max. Hertz Stress (GPa/ksi)	Test Time (Hrs.)	Remarks
1	4.1/600	0.1	Wear noted after 6 min. and several spalls had occurred.
2	5.5/800	1.0	Wear noted after 6 min. but run continued for 1 hr. by adjusting vibra switch to less sensitive position. Excessive wear and spalling occurred.
3	4.7/680	0.1	Excessive wear had occurred after 6 min.
4	4.1/600	1.0	Vibra switch set to insensitive position and test run for one hr. Gross wear and micro-spalling occurred.
5	4.5/680	0.15	Three areas spalled during 9 min. of testing.

TABLE 11

ROLLING FOUR-BALL TEST FATIGUE LIFE DATA ON 17.5 mm NORALIDE NC 132 Si_3N_4 BALLS

Spindle Ball Material	Ball Track (No.)	Spindle Speed (rpm)	Spindle Load (N/lbs)	Max. Hertz Stress (GPa/ksi)	Lundberg-Palmgren Computed L₁₀ Life (10^6 revs)	Test Time (hr.)	Equivalent Test Life at 800 ksi (10^6 revs)	Spindle Ball Condition After Test
NC 132	N-1	10,000	909/204	4.7/680	30	479		Unfailed
		10,000	1480/333	5.5/800	7	323	260	
NC 132	N-2	10,000	909/204	4.7/680	30	298		Spalled
		10,000	1480/333	5.5/800	7	182	251	
NC 132	N-3	10,000	909/204	4.7/680	30	374		Unfailed
		10,000	1480/333	5.5/800	7	283	222	
NC 132	N-4	10,000	909/204	4.7/680	30	304		Unfailed
		10,000	1480/333	5.5/800	7	316	232	
NC 132	N-5	10,000	909/204	4.7/680	30	158		Spalled
		10,000	909/204	5.5/800	7	0	22	
NC 132	N-6	10,000	909/204	4.7/680	30	367		Spalled
		10,000	1480/333	5.5/800	7	23	65	
NC 132	N-7	INVALID TEST DUE TO PROBLEMS WITH TEST RIG						
NC 132	N-8	INVALID TEST DUE TO PROBLEMS WITH TEST RIG						
NC 132	N-9	10,000	909/204	4.7/680	30	319		Spalled
		10,000	1480/333	5.5/800	7	34	65	
NC 132	N-10	10,000	909/204	4.7/680	30	310		Spalled
		10,000	1480/333	5.5/800	7	173	147	

TABLE 12

ESTIMATED SPALLING FATIGUE L_{10} LIFE VALUES FOR

<u>NORALIDE NC132</u> & <u>CERADYNE</u> 147Y SILICON NITRIDE BALLS

Material and Processing	Median Unbiased L_{10} Life Estimate	Median Unbiased Slope Estimate
NC132 Hot Pressed Spheres	33.07	1.12
NC132 Hot Pressed Billet	36.70	0.91
CER147Y Hot Pressed Spheres	15.00	1.30*
CVM M50 Steel	3.24**	1.48

* Assumed Weibull Slope

** The Lundberg-Palmgren computed L_{10} life for the M50 steel ball test load is 29×10^6 revs., whereas the computed L_{10} life for all the silicon nitride groups is 7×10^6 revs.

RESEARCH LABORATORY **SKF** INDUSTRIES, INC.

Norton   Ceradyne   GTE Sylvania
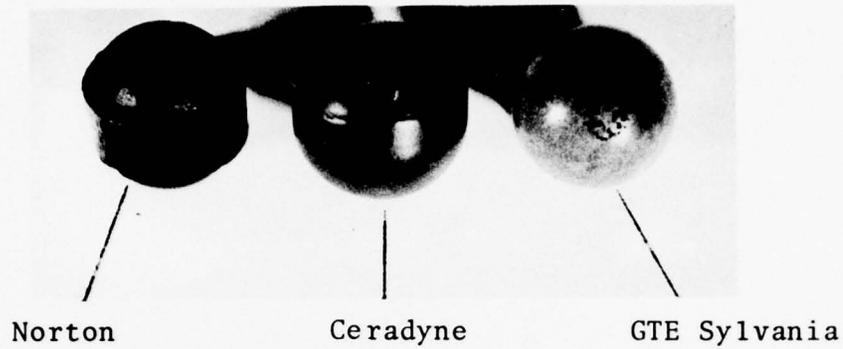
Figure 1.   Visual Comparison of Rough Silicon Nitride Spheres
            From Three Suppliers.

77-398   4X
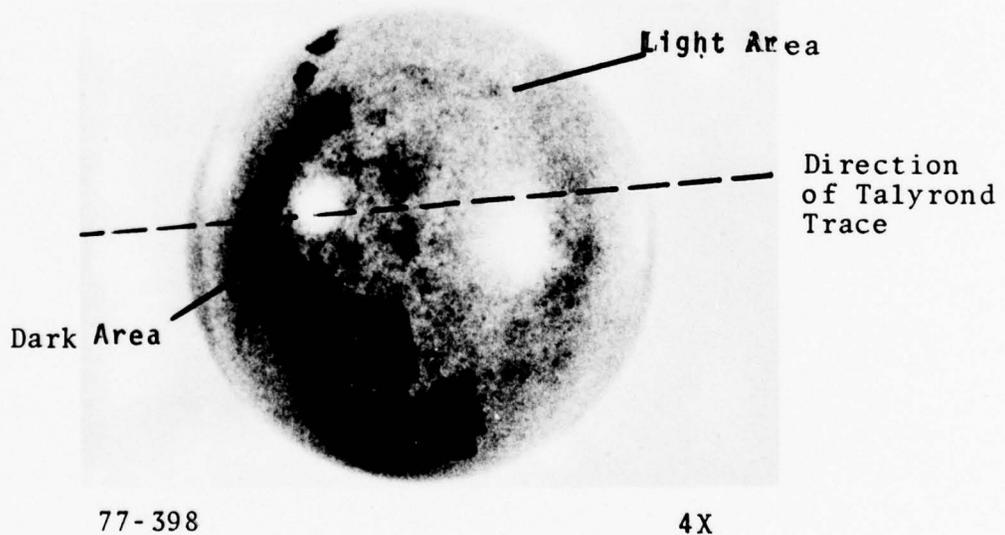
Figure 2.   Macrophotograph Showing Light and Dark Grey Areas
            on a Mottled GTE Sylvania Cold Pressed and Sintered
            Silicon Nitride Ball Which Has Poor Fatigue and
            Wear Life.

RESEARCH LABORATORY **SKF** INDUSTRIES, INC.
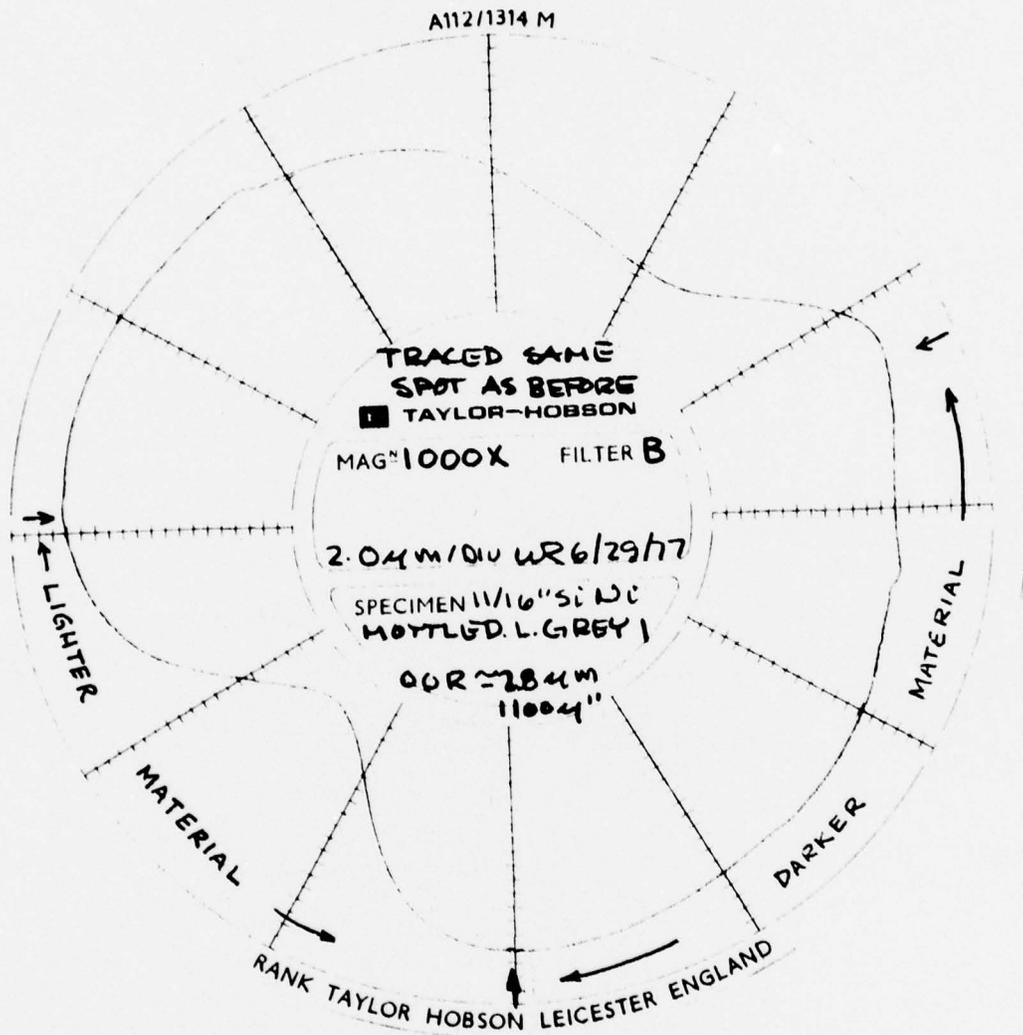
Figure 3.   Talyrond Trace on the Mottled GTE Sylvania Ball
            in Figure 2
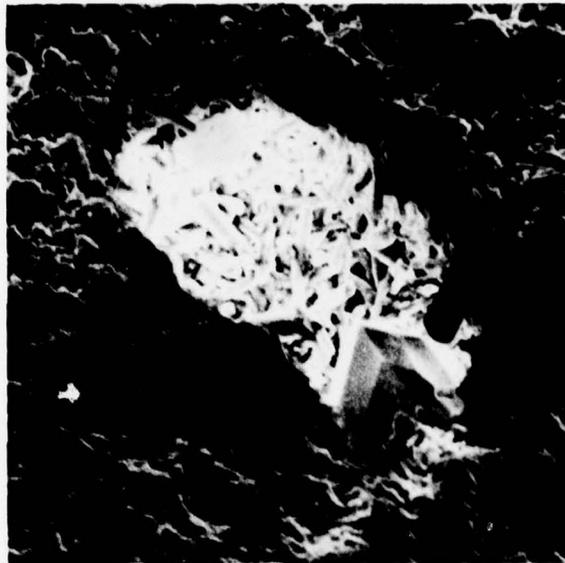
6435   1500X

(a) Light Area
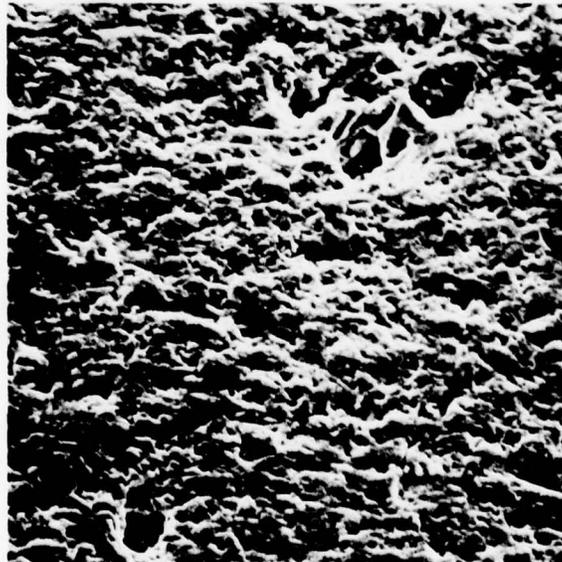
6434   1500X

(b) Dark Area

Figure 4.   Scanning Electron Micrographs Showing Difference in the Degree of Sintering Between Light and Dark Regions on a GTE Sylvania Ball Surface.
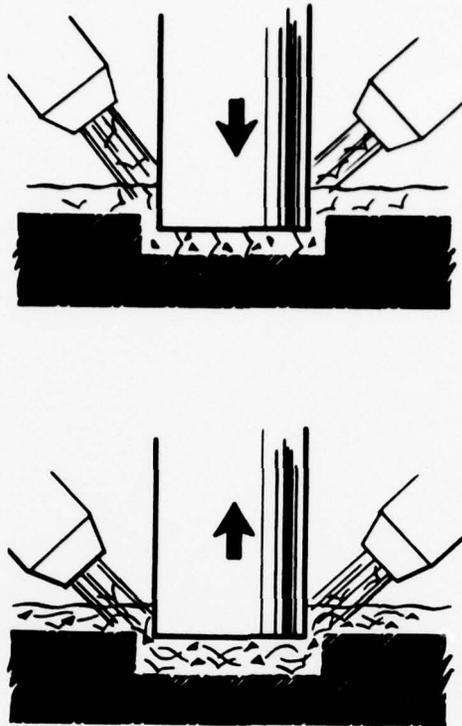
Figure 5.   Schematic Diagram of Ultrasonic Machining
Process Showing Flow of Abrasive Slurry
Between Workpiece and Vibrating Tool
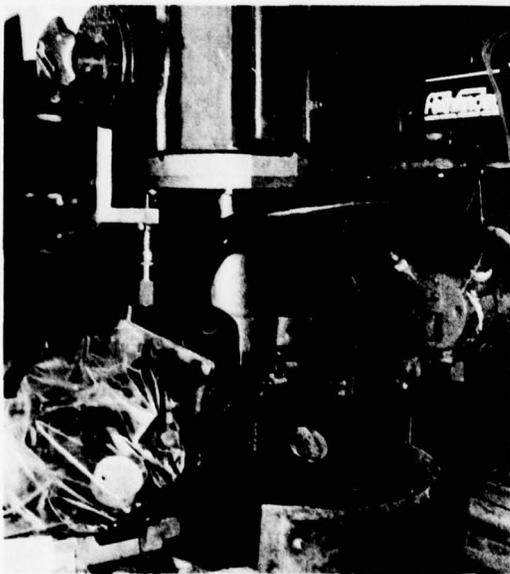
a) Machine in operation   b) View showing inner ring

Figure 6.   Ultrasonic Machining Set-Up for Ball Bearing
Inner Ring

RESEARCH LABORATORY **SKF** INDUSTRIES, INC.
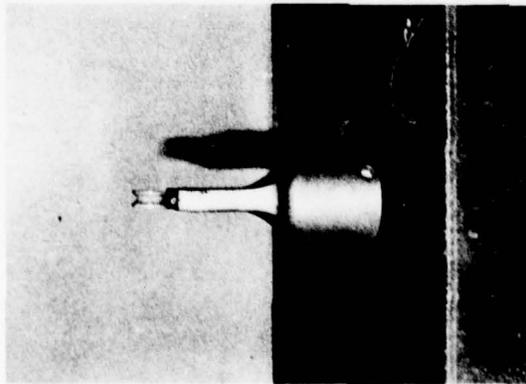
a) Inner Ring Groove Tool   b) Outer Ring Groove Tool   c) Outer Ring Counterbore Tool
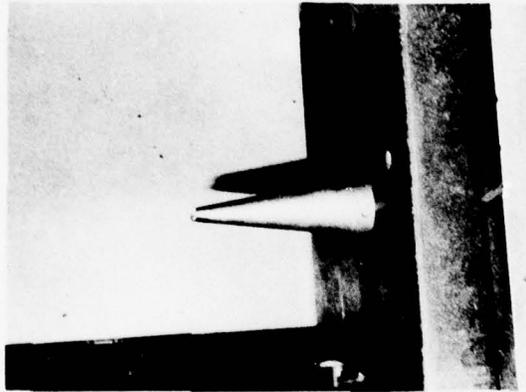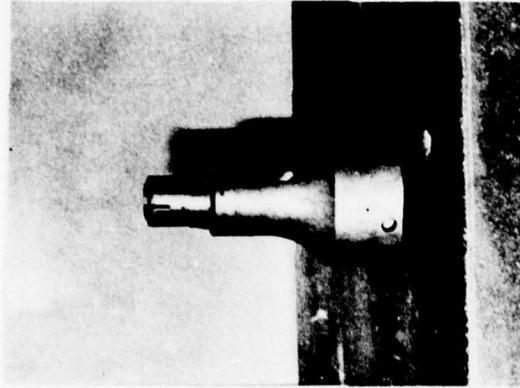
Figure 7. Ultrasonic Machining Tools for Producing the Outer Ring Bore and Both Inner and Outer Ring Grooves in Ball Bearing Rings
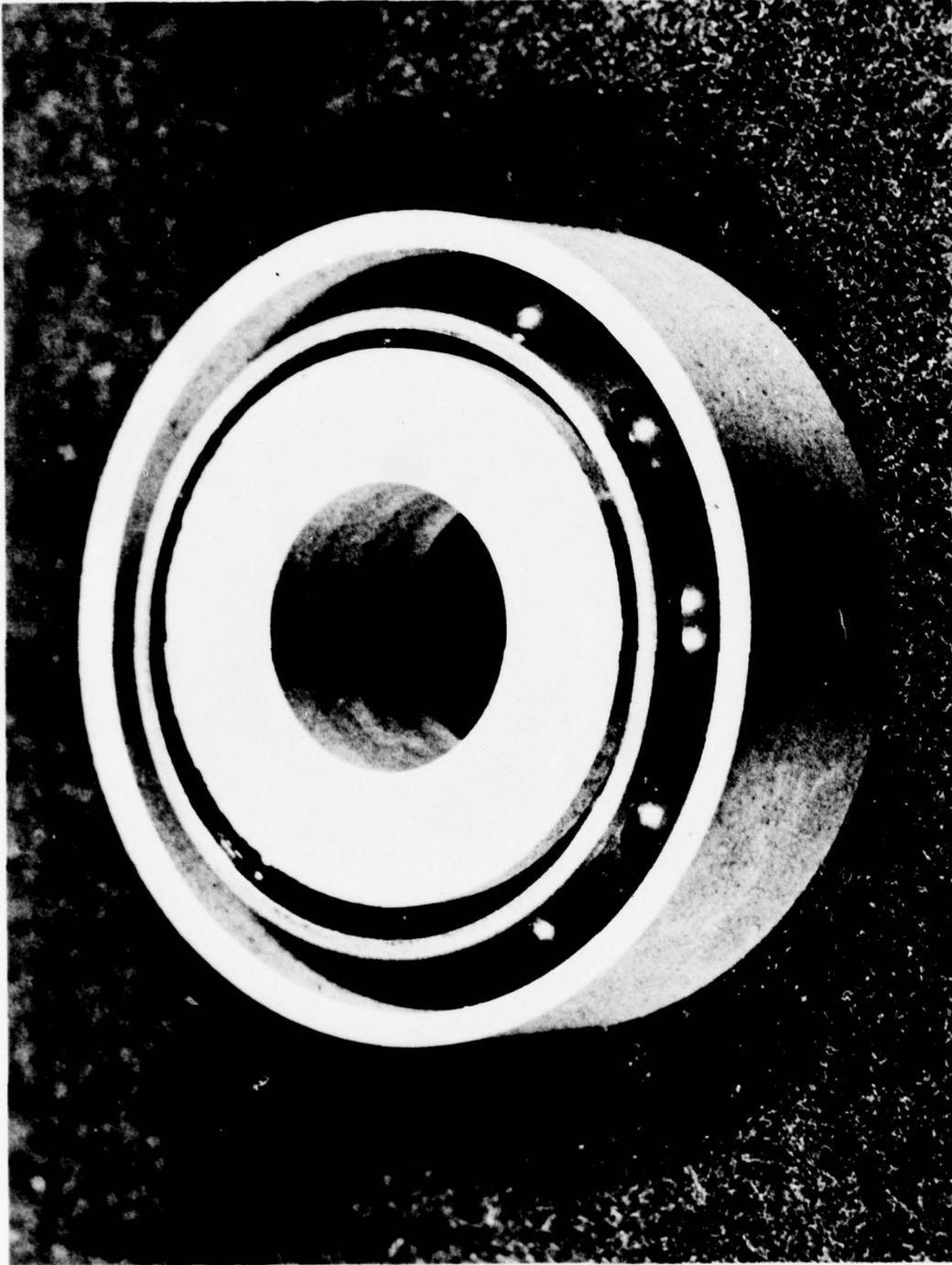
Figure 8. All-Silicon Nitride Turbine Bearing Manufactured by SKF With NC132 Hot Pressed Balls and Ultrasonically Machined Cold Pressed and Sintered Rings.

RESEARCH LABORATORY **SKF** INDUSTRIES, INC.
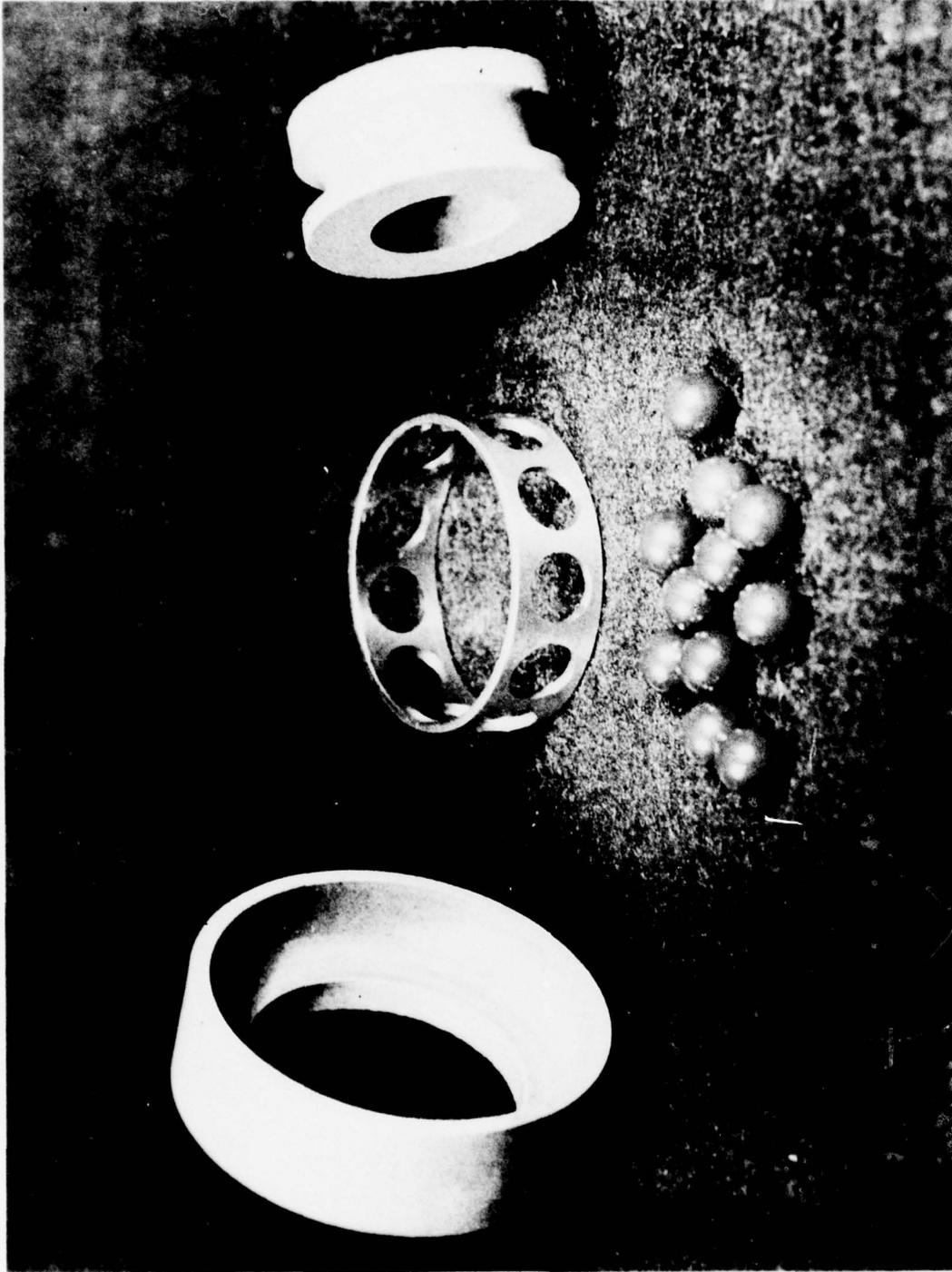
Figure 9. All-Silicon Nitride Turbine Bearing Components Manufactured by SKF Showing Ultrasonically Machined Ring Grooves and NC132 Hot Pressed Balls.

RESEARCH LABORATORY **SKF** INDUSTRIES, INC.
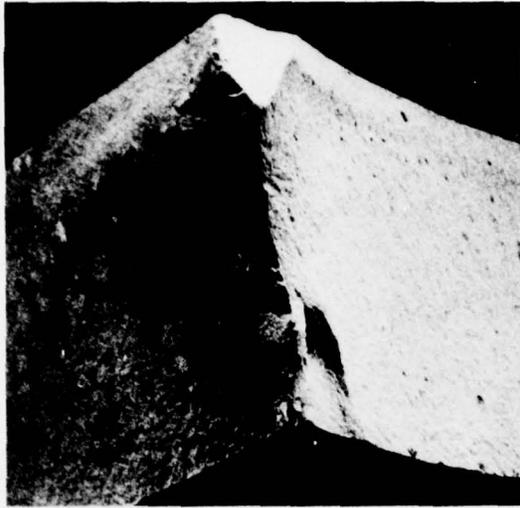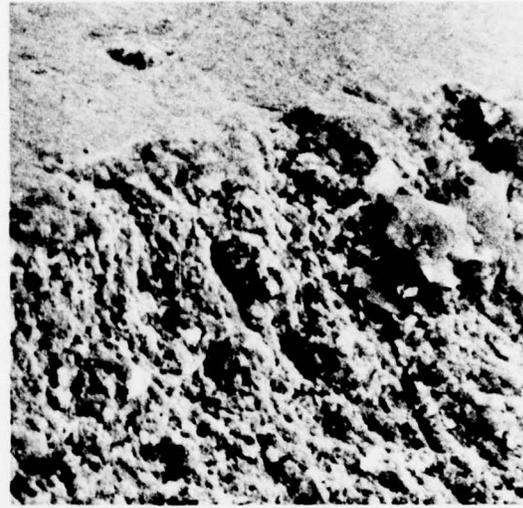
6417   50X   6418   1000X

Figure 10.   Fractograph of a Fractured GTE Sylvania Disc
              (0.43 GPa) Showing Fracture Initiation at a
              Pore.   Second Phase Inclusions (A) are visible
              at the Higher Magnification
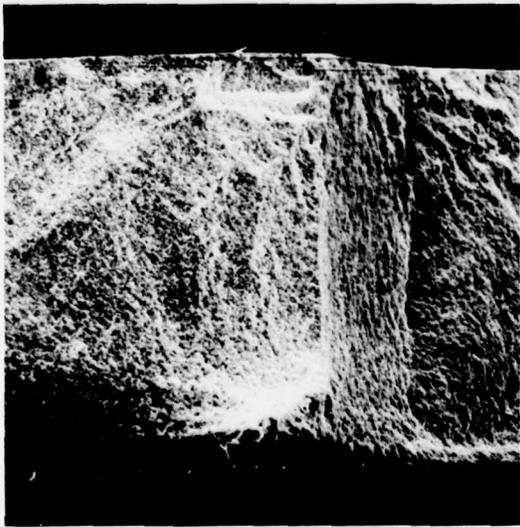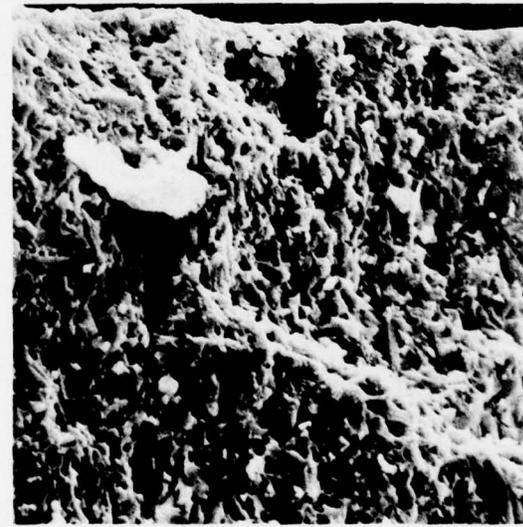
6419   50X   6420   1000X

Figure 11.   Fractograph of a Fractured Ceralloy 147Y Disc
              (0.56 GPa) Showing Fracture Initiation at a
              Second Phase Inclusion (B).
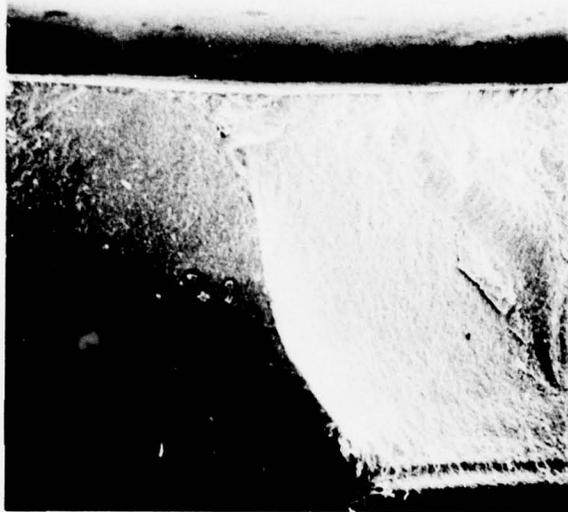
6421   50X

6423   250X

Figure 12.   Fractograph of a Fractured NC132 Disc (0.99 GPa)
              Indicating Fracture Initiation at Residual
              Surface Scratches.

RESEARCH LABORATORY **SKF** INDUSTRIES, INC.
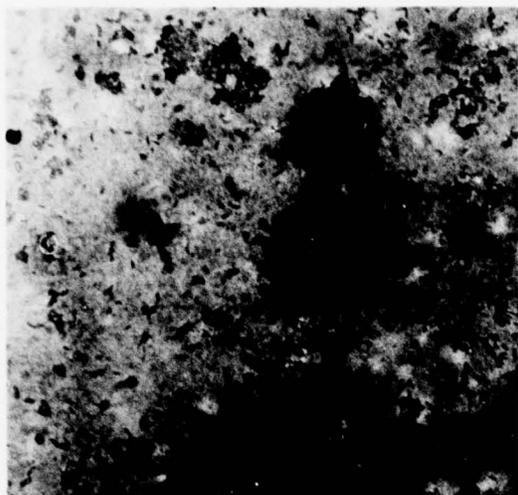
77-398   500X
Unpolarized Light
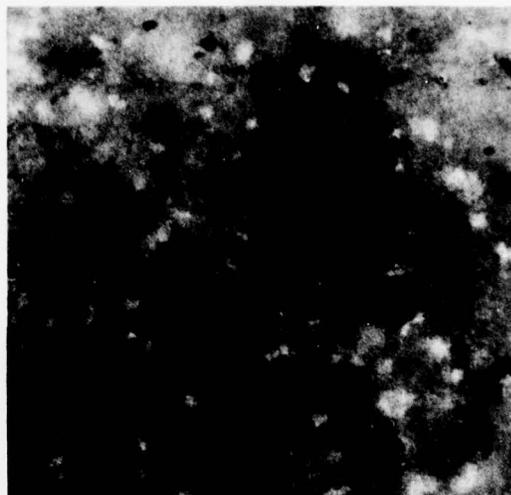
77-398   500X
Plane Polarized Light
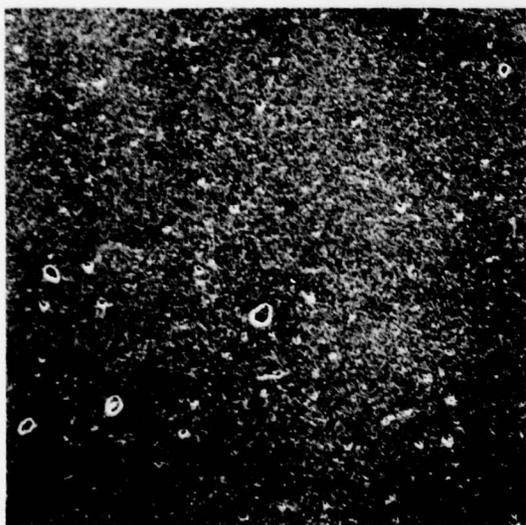
6294   100X
Secondary Electron Image
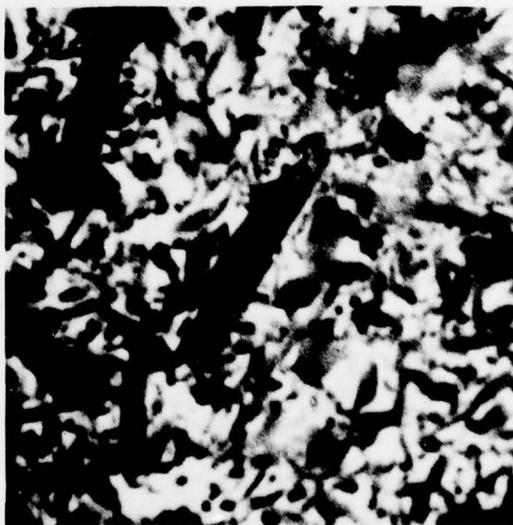
6295   5000X
Back-Scattered Electron Image

Figure 13.   Microstructure of Pressureless Sintered
GTE Sylvania Material from the Rough Sphere.
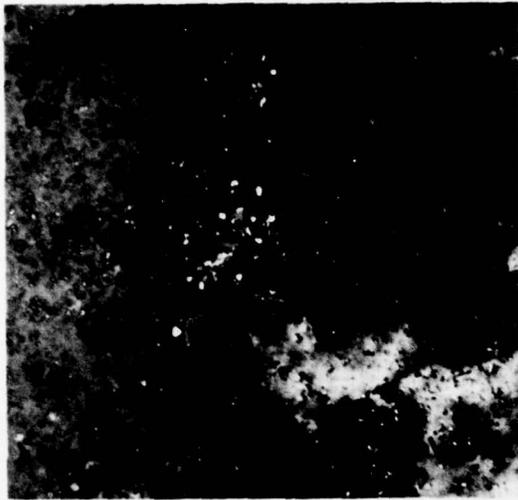
RESEARCH LABORATORY SKF INDUSTRIES, INC.

77-398   500X
Unpolarized Light
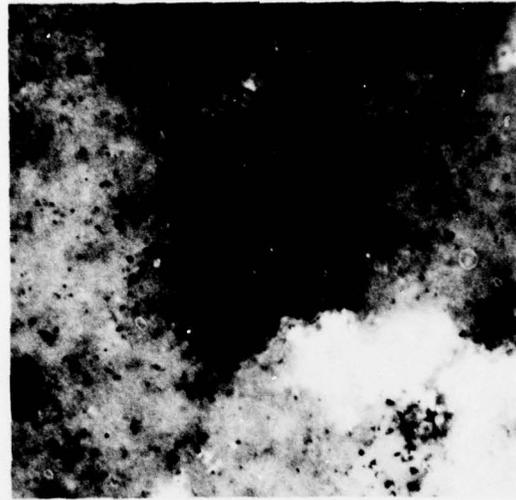
77-398   500X
Plane Polarized Light
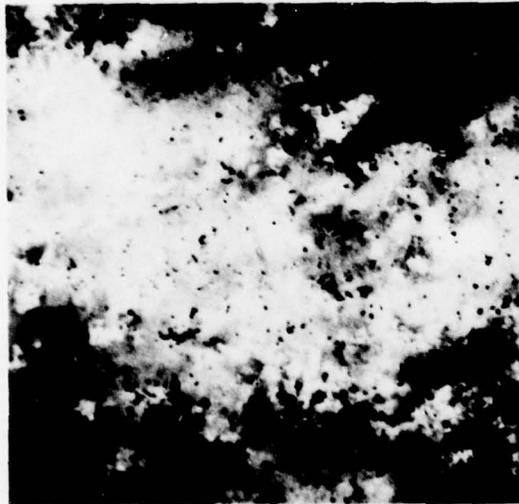
77-398   500X
Plane Polarized Light
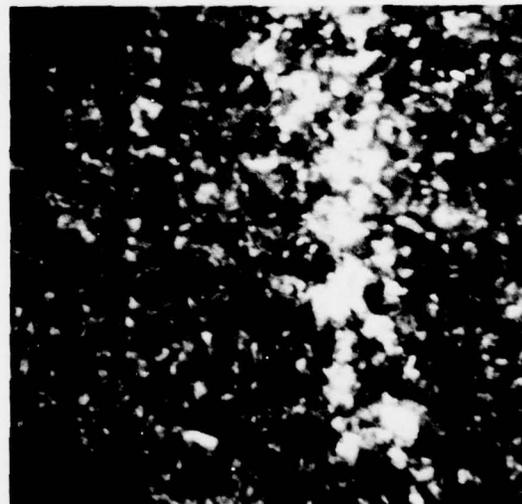
(d)   500X
Back-scattered Electron Image

Figure 14.   Microstructure of Ceralloy 147Y Material From a
              Ceradyne Hot Pressed Rough Sphere.   The Inclusions
              in (d) are rich in Yttrium.

RESEARCH LABORATORY **SKF** INDUSTRIES, INC.
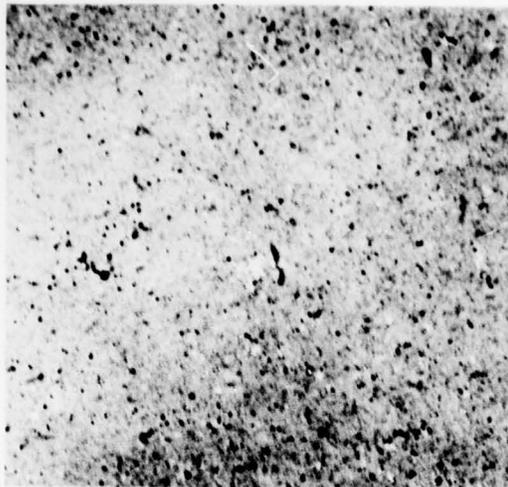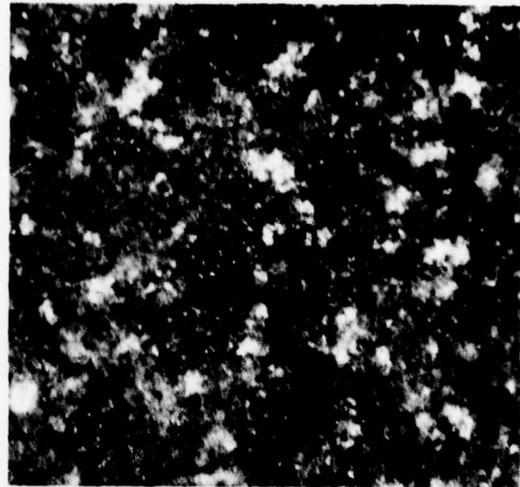
77-398   500X
Unpolarized Light
(a)

77-398   500X
Plane Polarized Light
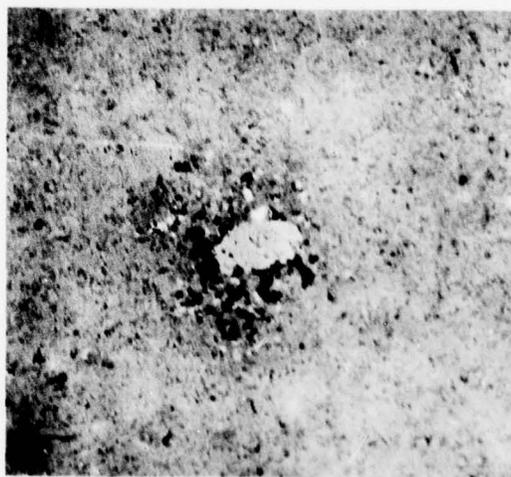
77-398   500X
(b) Old Norton

Figure 15. Microstructure of NC132 Grade Material From
            (a) Norton Hot Pressed Rough Sphere and
            (b) Older Norton Billet Material.

RESEARCH LABORATORY **SKF** INDUSTRIES, INC.

4888   5000X

Figure 16.   Backscattered Electron Image of NC132 Silicon
Nitride Ball Surface Showing Tungsten Rich ·
Segregation and Finish Processing Induced
Surface Microcracks Which Caused an Order of
Magnitude Reduction in Fatigue Life ·

77 398

77 39S
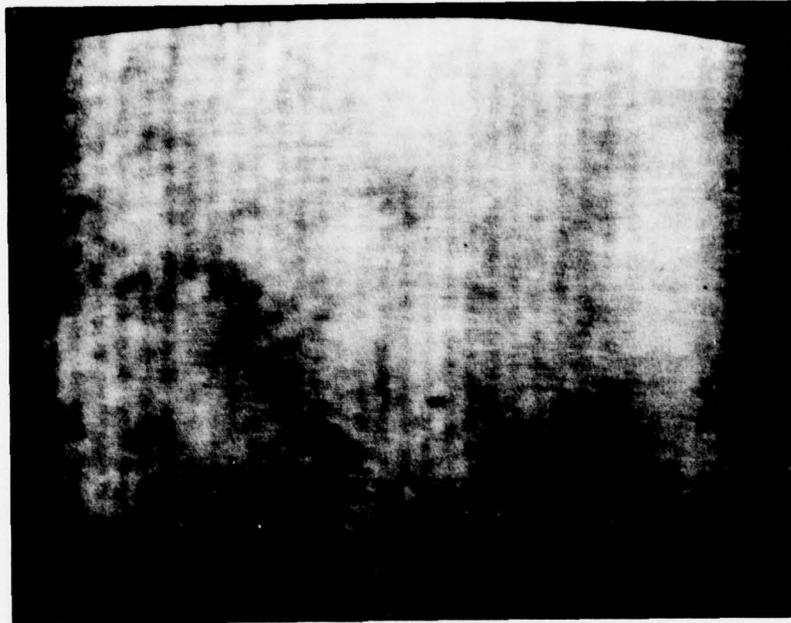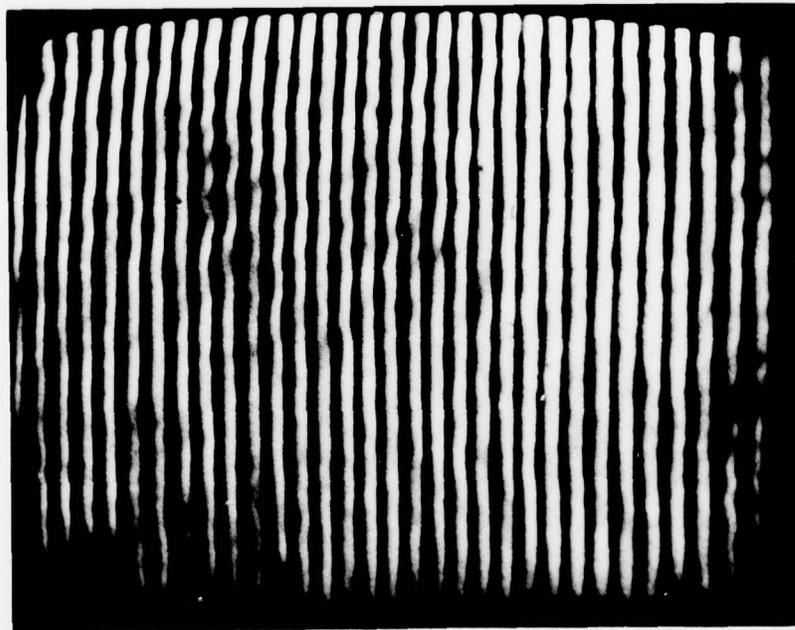
Figure 17. Transmission Acoustic Micrographs of a Section
From an NC132 Rough Sphere.

RESEARCH LABORATORY **SKF** INDUSTRIES. INC.

77 398
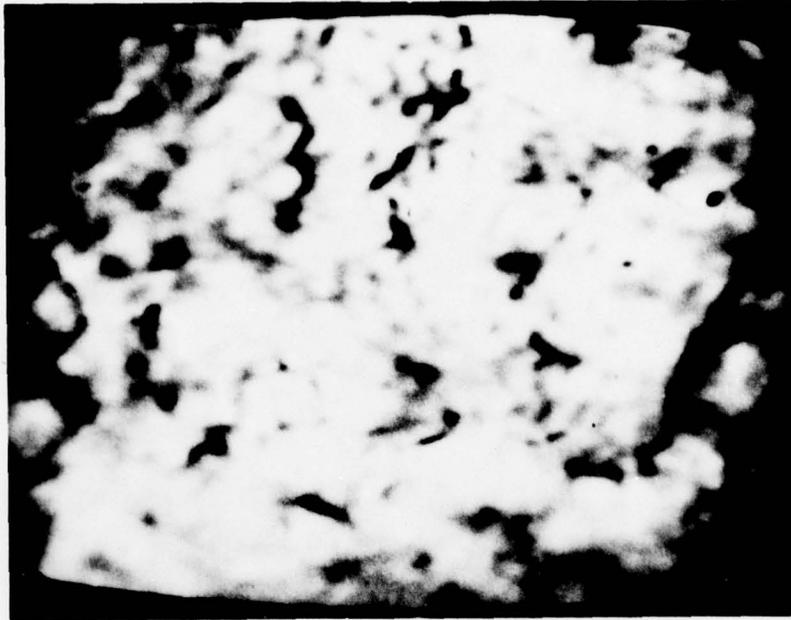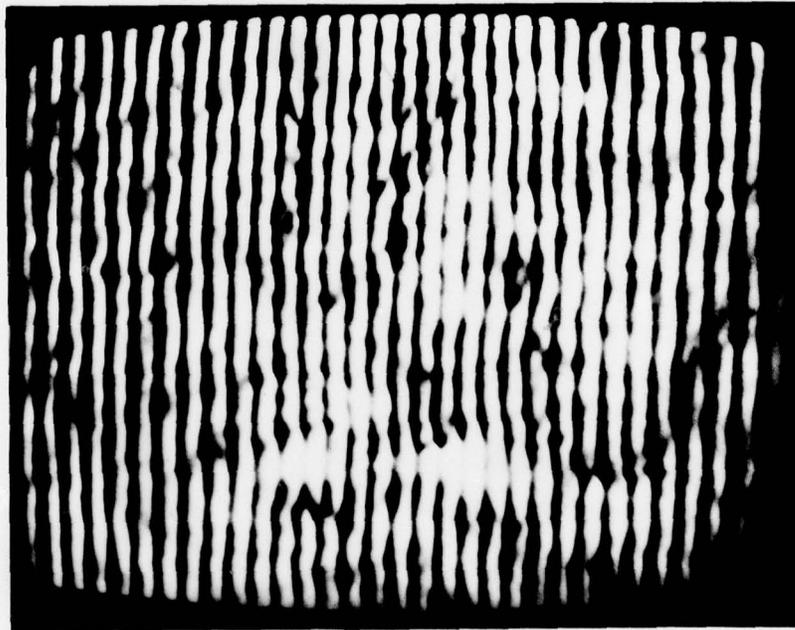
77 398

Figure 18. Transmission Acoustic Micrograph of a
Section From a Ceralloy 147Y Rough Sphere.

RESEARCH LABORATORY SKF INDUSTRIES. INC.

77 398
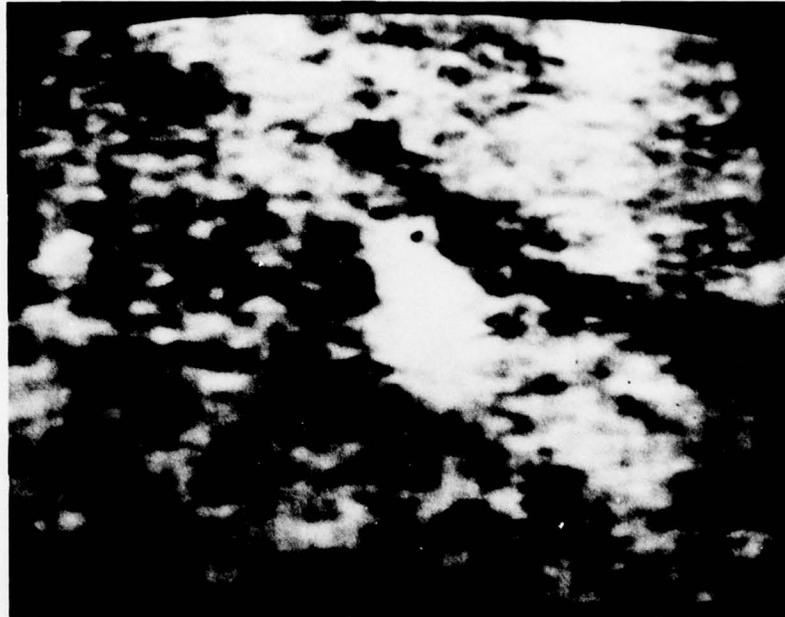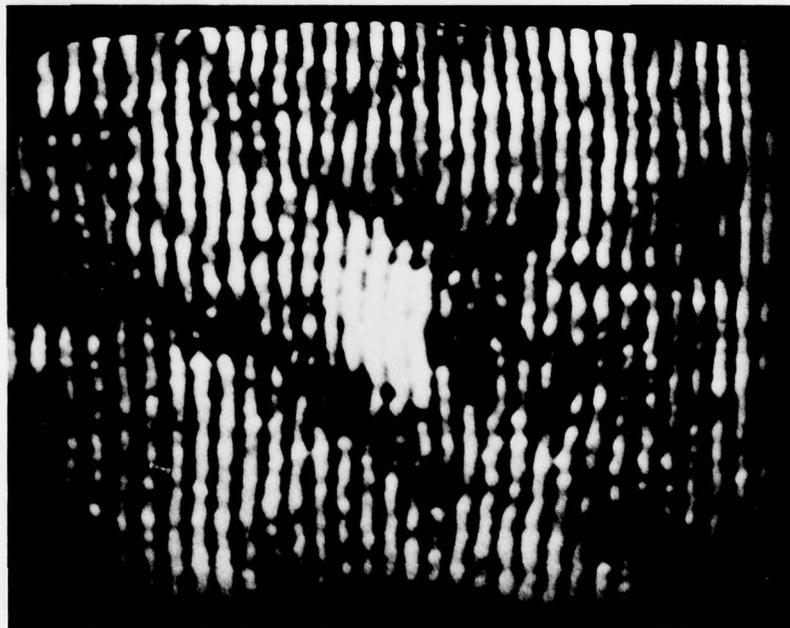
77 398

Figure 19. Transmission Acoustic Micrograph of a
Section From a GTE Sylvania Rough Sphere.

RESEARCH LABORATORY **SKF** INDUSTRIES, INC.
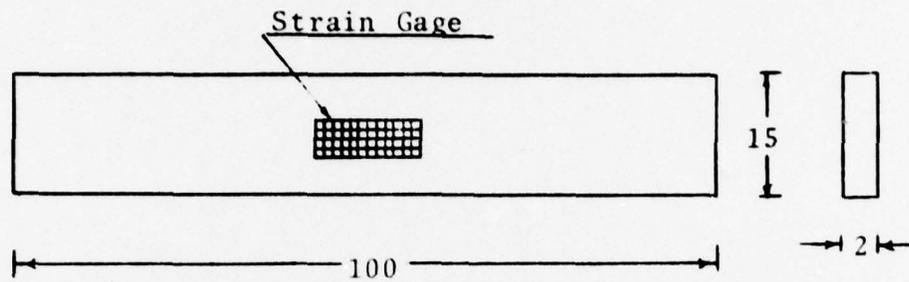
Figure 20. Schematic Showing a Strain Gaged Specimen For Calibration of X-ray Residual Stress Measurement Technique. Dimensions Are in mm.

(a)   4X

(b)   3X

Figure 21.   Photographs of Surfaces of (a) GTE Sylvania and (b) Norton Ball Produced by Krypton Exposure Technique. Dark (Exposed) Spots on the GTE Sylvania Ball are Indicative of Surface Porosity.
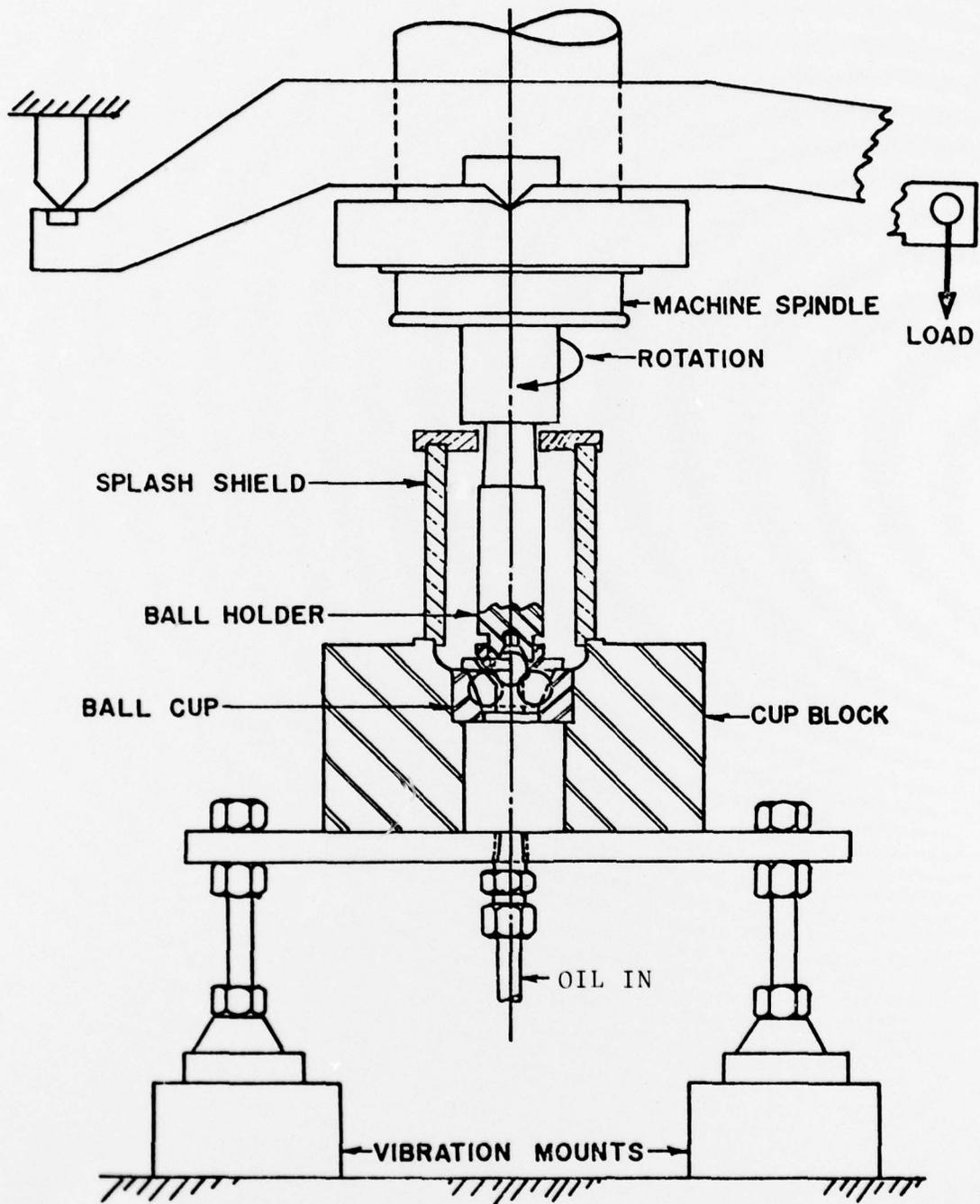
Figure 22.   Schematic Drawing of Rolling Four-Ball Tester

SPINDLE BALL (1)

SUPPORT BALLS (3)

CUP

α : CONTACT ANGLE
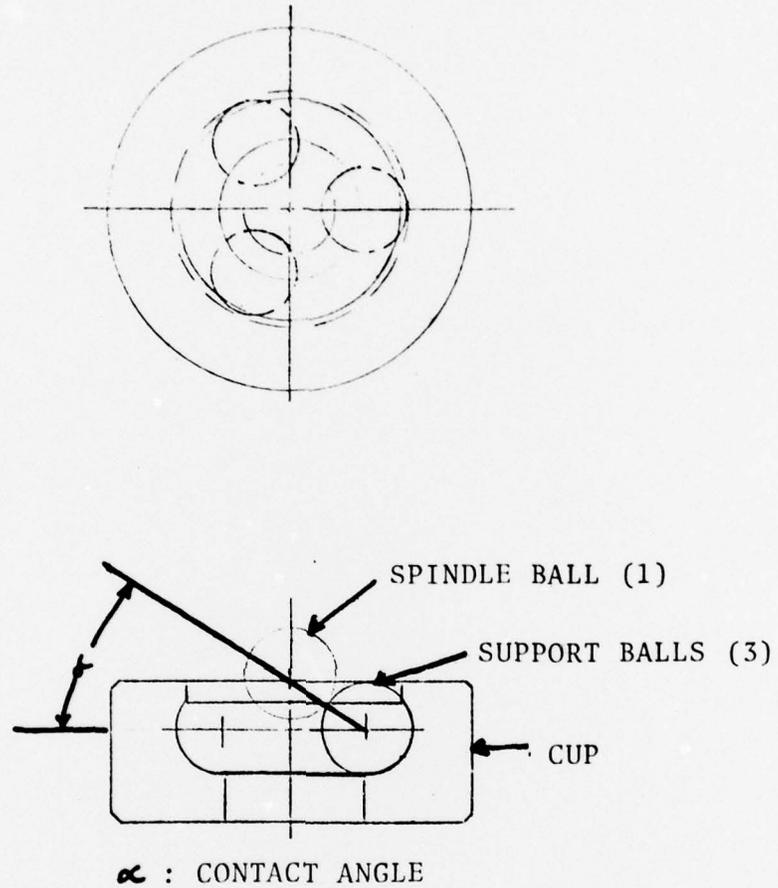
Figure 23. Schematic Drawing Showing the Relative Positions
of Test and Support Balls

RESEARCH LABORATORY SKF INDUSTRIES, INC.
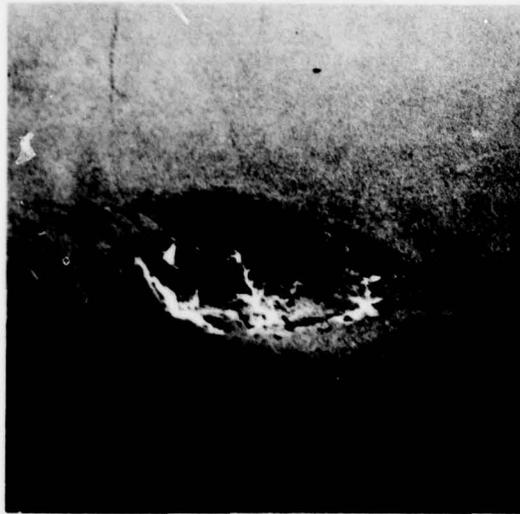
6424   30X

Figure 24.   Normal Fatigue Spall on an NC132 Ball.
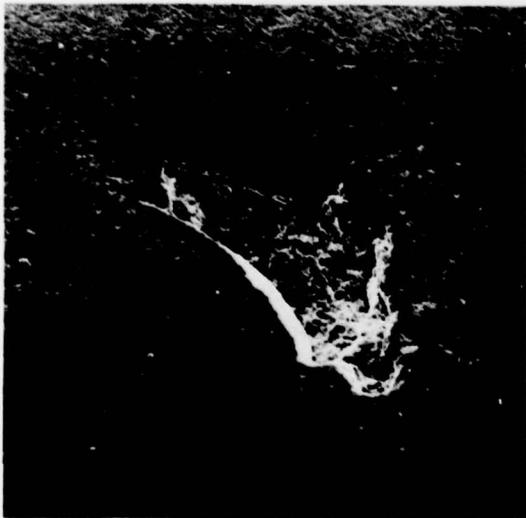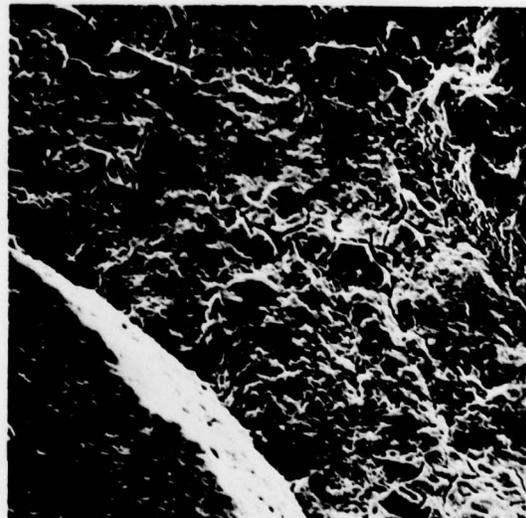
6430   125X   6431   500X

Figure 25.   Fatigue Spall Caused Due to Repeated Contact
with Spalls on Support Balls.

RESEARCH LABORATORY **SKF** INDUSTRIES, INC.
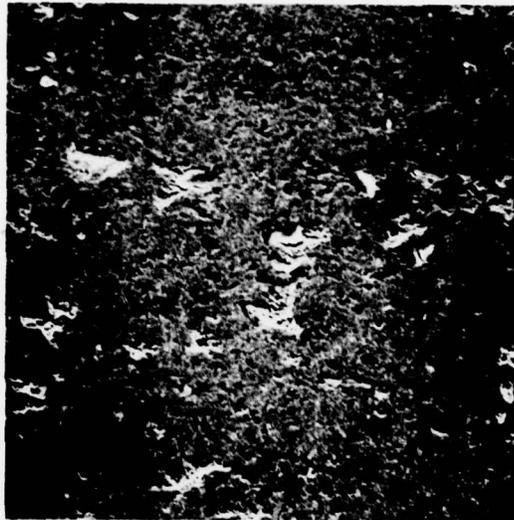
6433   500X
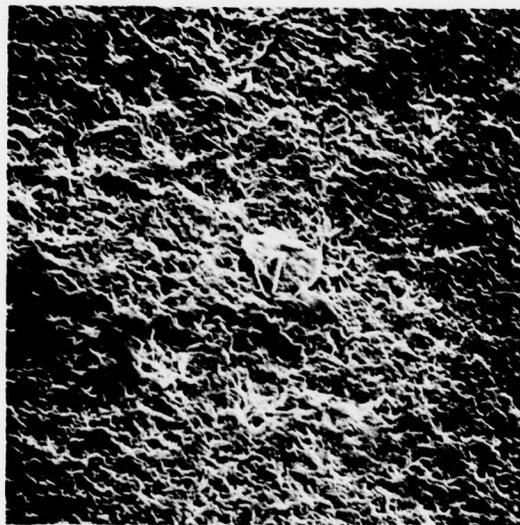
6429   500X

Figure 26.   Microspalls and Wear Debris Found on a Fatigue
             Tested Ceralloy 147Y Ball.

RESEARCH LABORATORY **SKF** INDUSTRIES. INC.